POLITECNICO
MILANO 1863

Department of Civil and Environmental Engineering
Master of Science in Environmental and Land Planning Engineering

---

AN INVESTIGATION OF TURBIDITY AND ABSORBANCE EFFECT ON UV DISINFECTION PERFORMANCE FOR WATER AND WASTEWATER TREATMENT

Supervisor:
Dr. Andrea Turolla

Master's Thesis by:
Ali Amini

Academic Year 2020-2021

ACKNOWLEDGMENTS

I would like to express my sincere gratitude to my esteemed supervisor Dr. Andrea Turolla for providing me with all the resources needed to complete my thesis, as well as his continuous support, advice, and patience at every stage of this research project. His immense knowledge and plentiful experience have encouraged me in all the time of my academic research, and the completion of this thesis could not have been possible without his expertise.

I also would like to offer my special thanks to Jacopo Foschi for his support in my lab work. My special thanks are extended to my lab mates and the Laboratory of Environmental Engineering (LIA) staff at Politecnico di Milano.

I am extremely grateful to my parents for their love, caring, and sacrifices for educating and preparing me for my future. Without their tremendous support and encouragement, it would be impossible for me to complete my study. Also, I express my thanks to my brother and my sister for encouraging me throughout this research work.

ABSTRACT

In water and wastewater treatment systems, turbidity and absorbance are well-recognized as factors that can affect ultraviolet (UV) disinfection performance, resulting in less efficient pathogen inactivation. However, further studies are required to improve the description in a quantitative way to enhance engineering applications based on UV disinfection. This study aims at (i) investigating the turbidity and absorbance effect on UV inactivation of *Escherichia coli* (*E. coli*) in three different sample depth conditions (1, 2.5, and 4 cm) using a standard bench-scale collimated beam (CB) apparatus, (ii) modeling the effect of turbidity and absorbance on UV radiation in CB apparatus, and (iii) modeling the turbidity and absorbance effect on *E. coli* and MS2 inactivation in a small-scale UV disinfection reactor. A computational fluid dynamics (CFD) software was used for both modeling activities. *E. coli* inactivation experiments and the obtained general linear model (GLM) indicated the significant effect of turbidity, absorbance, and their interaction on UV disinfection. Moreover, the inactivation rate decreased by increasing the sample depth from 1 to 4 cm for the same applied UV dose and optical properties. The *E. coli* dose-response curve in sample depth of 4 cm was effectively described by a linear regression model characterized by an inactivation rate constant of 0.67 cm^2/mJ. The results of relative corrected UV doses and relative inactivation rates obtained from GLM indicated the need for another correction factor to consider the scattering effect caused by turbidity. However, the CB apparatus modeling results were not accurate enough to use the simulated average radiation for determining a related-turbidity correction factor. UV disinfection reactor modeling results indicated that the effect of absorbance on microbial inactivation was prevalent with respect to turbidity. According to reactor modeling results, high UV doses were applied in the UV disinfection reactor, resulting in *E. coli* complete inactivation, unlike MS2. CFD simulations could effectively predict inactivation results for MS2 obtained during field experiments on two real water matrices.

ABSTRACT

Nel trattamento delle acque, la torbidità e l'assorbanza sono fattori noti per influenzare le prestazioni della disinfezione con radiazione ultravioletta (UV), condizionando negativamente le efficienze di inattivazione. Tuttavia, ulteriori studi sono necessari ad approfondire la conoscenza di tali fenomeni per migliorare le applicazioni ingegneristiche. Questo studio mira a (i) indagare l'effetto di torbidità e assorbanza sull'inattivazione di *Escherichia coli* (*E. coli*) in tre diverse condizioni di spessore del campione (1, 2,5 e 4 cm) utilizzando un apparato di irraggiamento a radiazione collimata (CB) da banco (ii) modellare l'effetto della torbidità e dell'assorbanza sulla radiazione UV nell'apparato CB, e (iii) modellare l'effetto di torbidità e assorbanza sull'inattivazione di *E. coli* e MS2 in un reattore di disinfezione UV a piccola scala. La modellazione è stata condotta con un software di fluidodinamica computazionale (CFD). Gli esperimenti di inattivazione di *E. coli* e il modello lineare generale (GLM) ottenuto hanno indicato l'effetto significativo di torbidità, assorbanza e della loro interazione sulla disinfezione UV. Inoltre, il tasso di inattivazione è diminuito aumentando la profondità del campione da 1 a 4 cm a parità di dose UV applicata e proprietà ottiche. La curva dose-risposta di *E. coli* in campioni di spessore 4 cm è stata efficacemente descritta da un modello di regressione lineare caratterizzato da una costante del tasso di inattivazione di 0.67 cm^2/mJ. L'analisi dei dati sperimentali ha indicato la necessità di un ulteriore fattore di correzione per considerare l'effetto di diffusione causato dalla torbidità, seppur i risultati della modellazione dell'apparato CB non si siano mostrati sufficientemente accurati per determinare tale fattore. I risultati della modellazione del reattore UV hanno evidenziato che l'effetto dell'assorbanza sull'inattivazione microbica è prevalente rispetto alla torbidità. Le dosi UV stimate dal modello hanno predetto la completa inattivazione di *E. coli*, a differenza di MS2. Infine, le simulazioni sono state efficaci nel predire l'inattivazione su MS2 ottenuta in esperimenti di campo su due matrici acquose.

TABLE OF CONTENTS

LIST OF TABLES

LIST OF FIGURES

LIST OF ABBREVIATIONS

A_{254}	Absorbance at Wavelength of 254 nm
CB	Collimated Beam
CFD	Computational Fluid Dynamics
CFU	Colony Forming Unit
DBPs	Disinfection by-Products
DI	Deionized
DO	Discrete Ordinate
E. coli	*Escherichia coli*
GLM	General Linear Model
LB	Liquid Broth
LED	Light Emitting Diode
LP	Low Pressure
LR	Linear Regression
MP	Medium Pressure
NTU	Nephelometric Turbidity Unit
RTE	Radiative Transfer Equation
TCMs	Turbidity-Causing Materials
USEPA	U.S. Environmental Protection Agency
UV	Ultraviolet
UVT	UV transmittance

CHAPTER 1. INTRODUCTION

Ultraviolet (UV) light has gained growing acceptance as a disinfection process for water and wastewater disinfection due to its broad-spectrum efficiency against various pathogens and non-formation of disinfection by-products (DBPs) (Hijnen et al., 2006). By the use of UV radiation, a variety of water types such as secondary and tertiary wastewater effluents, stabilization ponds, combined sewer overflows as well as filtered and unfiltered surface waters, and groundwaters can be disinfected (Mamane, 2008).

On the one hand, due to the extremely high UV absorbance of biological flocs that are formed during secondary treatment in wastewater treatment plants, pathogens may be harbored and shielded from exposure to UV radiation by these biological flocs, resulting in reducing the performance of UV disinfection (Azimi et al., 2012; Emerick et al. 1999). On the other hand, in water resources, particles can decrease the effectiveness of UV disinfection mainly by shielding, scattering, absorbing, or blocking UV radiation, hence protecting the embedded microorganisms from UV radiation (Wu et al. 2005).

Although many research projects (Farrell et al., 2018, Mamane et al., 2006; Passantino et al., 2004; Batch et al., 2004; Christen and Linden, 2003) have been undertaken to examine the effect of turbidity and absorbance on UV disinfection in water and wastewater systems, a better understanding of the influence of these parameters on UV disinfection performance is therefore needed to investigate the behavior of UV radiation in different water depths and water matrices as a function of various optical properties to assess whether the proposed corrections in literature are sufficient. This could be conducted by considering a statistical analysis of experimental data and simulations, using computational fluid dynamics (CFD) tools that involve multiple phenomena in order to improve the description in a better quantitative way, resulting in more accurate modeling of UV disinfection reactor, which plays a vital role in pathogen inactivation.

This research work is divided into a laboratory experimental activity task and UV disinfection modeling tasks performed by commercial CFD software. To be more precise, this study aims at (i) assessing the effect of water quality parameters, including turbidity and absorbance, on UV disinfection performance by testing an important microbiological indicator, *Escherichia coli* (*E. coli*), utilizing a bench-scale collimated beam (CB) apparatus equipped with a low-pressure (LP) mercury lamp, irradiating water samples at different depths

of 1, 2.5, and 4 cm to determine the UV dose-response curves, (ii) modeling of the CB apparatus under the effect of turbidity and absorbance to investigate the optical behavior of different water matrices in the CB apparatus, obtaining accurate average UV irradiance throughout the samples under different conditions, (iii) modeling of a small-scale UV disinfection reactor for the household water treatment to investigate the effect of water quality parameters in the simulated UV disinfection reactor and compare the predicted log inactivation with experiments.

Concerning the structure of the thesis, a review of previous literature, methodologies followed, results and discussion, research conclusions, and ideas for furthering research are covered in the chapters found in this present work. In detail, in Chapter 2, a general overview on the subject of the UV disinfection process, UV radiation sources, related definitions, the mechanism of microorganism inactivation and repair with the related kinetic model, as well as a literature review of factors affecting UV disinfection performance are provided. The methodologies and procedures for the experimental plan are discussed in Chapter 3, including UV inactivation experiments, UV disinfection modeling, and materials used. Results and discussion obtained from this work are addressed in Chapter 4. Finally, research conclusions and future research recommendations can be found in Chapter 5.

CHAPTER 2. STATE OF THE ART

This chapter provides a general overview of UV disinfection for water and wastewater treatment (Section 2.1), UV radiation sources (Section 2.2), a thorough description of relevant definitions (irradiance, fluence rate, and UV dose) (Section 2.3), the mechanism of microorganism inactivation and repair (Section 2.4), UV dose-response and related kinetic model (Section 2.5) as well as describing factors affecting UV disinfection performance (Section 2.6).

2.1 UV Radiation in Water and Wastewater Disinfection

Disinfection is an essential step in water and wastewater treatment that ensures water is safe to use. The disinfection process either inactivates or kills pathogenic microorganisms (bacteria, fungi, parasites, etc.) through the application of disinfecting agents (Gelete et al., 2019). Some of the most popular methods that can be successfully used to disinfect water and wastewater are chlorination, ozonation, and UV radiation (Crittenden et al., 2012; Metcalf and Eddy, 2003).

Chlorination has been one of the most widespread disinfection techniques used in water and wastewater treatment plants since chlorine-based disinfectants are relatively inexpensive (Chawla et al., 2015). However, the drawbacks of chlorination such as the foul odor and taste, ineffectiveness against protozoa eggs and cysts, the trihalomethanes and other types of chlorination by-products formation, have prompted the introduction of other disinfection techniques (Zhai et al., 2017).

Another popular disinfection agent that is used instead of chlorine is ozone. Compared to chlorine, it is an extremely effective disinfectant that quickly oxidizes chemical residuals, pesticides, various pathogens, and organic matter in short contact times and low concentrations (Rosenblum et al., 2012). The main drawback is associated with the possibility of producing dangerous by-products during the partial oxidation of dissolved organic compounds (Xi et al., 2017). In addition, ozone production for wastewater disinfection applications may not be cost-effective due to the high-energy costs associated with ozone generation (Orta de Velasquez et al., 2008).

UV radiation is another widespread technique that is used for the disinfection of water and wastewater. Johann Ritter was the first person who discovered UV light in 1801. After

establishing the germicidal effect of UV light on bacteria, using it in the treatment of *Lupus vulgaris* (a form of tuberculosis) by Niels Finsen in 1900, mercury lamps development as artificial UV light sources in 1901, founding the most effective wavelength (around 250 nm) for inactivation of bacteria by Bernard and Morgan in 1903 and the use of quartz as a UV transmitting material in 1906, UV radiation was used for the first time in 1910 to disinfect drinking water in Marseilles (Gray, 2014; Bolton and Cotton, 2008; Hijnen et al., 2006; USEPA, 2006). According to Wolfe (1990) and Hoyer (2004), due to high costs, poor equipment reliability, maintenance problems, and the advent of chlorination (cheaper, more reliable, and potential to measure disinfectant residual), the general application of UV radiation was impeded, but as more information gained on the production of hazardous oxidation by-products during chlorination and ozonation, UV disinfection became more popular (Hijnen et al., 2006). In addition, in the past years, due to considerable advances in technology, UV disinfection has emerged as one of the best water treatment options available, particularly in North America and Europe, adopting UV as the main disinfection process (Kheyrandish et al., 2018).

Unlike chlorine and ozone that are based on chemical agents, UV disinfection is a physical process. Due to its nature, UV radiation has several benefits and drawbacks when compared to chemical disinfectants.

2.1.1 Advantages of UV Disinfection

- UV radiation is an effective disinfectant, and it does not significantly change the quality of water. That is, no changes in DBPs formation potential, smell, turbidity, pH, and TOC occur during the process (Bolton and Cotton, 2008; Dotson et al., 2012; Gelete et al., 2019);
- It is extensively used as a disinfectant in water treatment due to its capacity to inactivate a broader range of disease-causing microorganisms, including *Giardia cysts* and *Cryptosporidium oocysts* (Betancourt and Rose, 2004);
- As the contact time needed to effectively inactivate the pathogens using UV radiation is in the range of a few seconds, UV disinfection is a rapid process; and
- It can be easily operated (i.e., turn up or turn down) based on the changes in water flow, water quality, etc. (Bolton and Cotton, 2008).

2.1.2 Disadvantages of UV Disinfection

- UV disinfection inactivates microorganisms through the damage of their DNA, but some microbes are able to repair it via either photoreactivation or dark repair mechanism, which allows inactivated microorganisms to re-contaminate water (Sousa et al., 2017; Rodriguez et al., 2014; Hijnen et al., 2006);
- The microbiological stability in the distribution systems cannot be guaranteed by UV radiation since it does not provide any residual disinfection effect (Choi and Choi, 2010);
- Fouling material accumulation on the UV lamp quartz sleeves reduces the performance of UV disinfection; thus, regular cleaning of the quartz sleeves is needed to maintain adequate disinfection (Bolton and Cotton, 2008; Emerick et al., 1999);
- UV lamps degrade as they age, leading to a decrease in output that causes a drop in UV dose delivery over time. Thus, periodical check of UV lamps operation is required (USEPA, 2006).

2.2 UV Radiation Sources

UV light is the part of electromagnetic radiation spectrum between X-rays and visible light (Figure 2.1), and it covers the wavelength ranging from 100 to 400 nanometers (nm). This region is divided into vacuum UV (100-200 nm), UV-C (200- 280 nm), UV-B (280- 315 nm), and UV-A (315- 400 nm) (USEPA, 2006). However, not all the wavelengths of UV light are equally effective at inactivating microorganisms. It is known that UV radiation only has germicidal effects in the wavelengths found under the UV-C and UV-B spectrum; more particularly, the maximum germicidal effect of UV light occurs at the single wavelength of 253.7 nm (Reed, 2010).

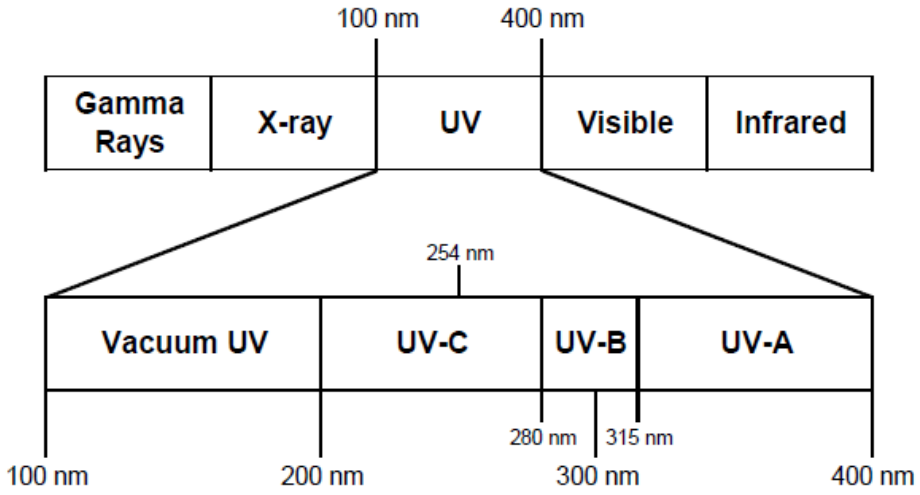

Figure 2.1: Electromagnetic spectrum (U.S. Environmental Protection Agency (USEPA), 2006).

In conventional UV sources, it is needed to apply a voltage across a gas mixture for generating UV light, which leads to a photon discharge. The specific wavelengths of light emitted from the discharge of photons rely on the elemental composition of the gas and the power level of the lamp (USEPA 2006). The most common UV sources for current UV disinfection systems are LP and medium-pressure (MP) mercury lamps. As seen in Figure 2.2, LP lamps have monochromatic emission at a wavelength of 253.7 nm, while MP lamps have polychromatic emission light at a broad range of wavelengths, from 200 to 600 nm (Beck, S.E. et al., 2015; Bolton and Cotton, 2011). Emerging UV source, termed UV light-emitting diode (UV-LED), has been developed with many special features and advantages, such as being free from mercury, low power requirements, and various wavelength diversity through various combinations of semiconductor materials (Song et al., 2016).

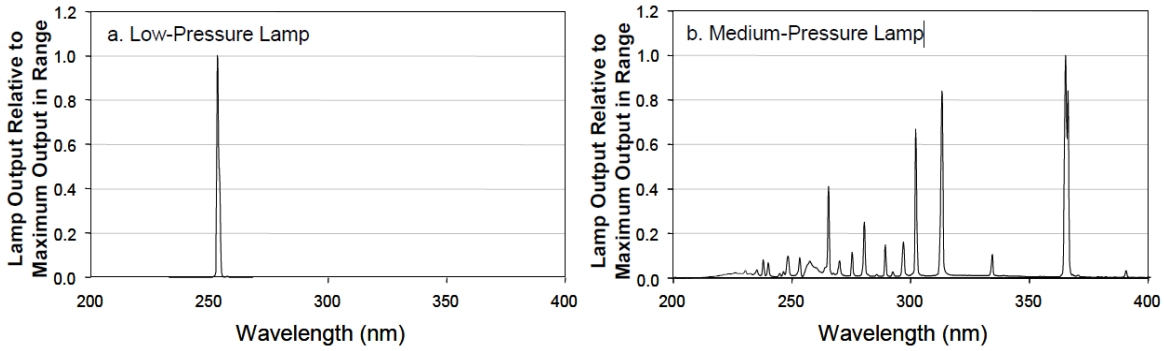

Figure 2.2: (a) UV output of LP and (b) MP mercury vapor lamps (USEPA, 2006).

2.3 Irradiance, Fluence rate and UV Dose Definition

UV irradiance or intensity is a fundamental property of UV radiation and has the units of watts per meter squared (W/m^2) (USEPA, 2006). UV Irradiance and fluence rate are two different terms in which the first one is defined as the total radiant power incident from all upward directions on an infinitesimal element of the surface of area dA containing the point under consideration divided by dA while the second one is defined as the total radiant power incident from all directions onto an infinitesimally small sphere of cross-sectional area dA, divided by dA. (Bolton and Linden, 2003). In a well-designed bench scale setup such as CB apparatus (Figure 2.3), UV irradiance and fluence rate are expected to be the same.

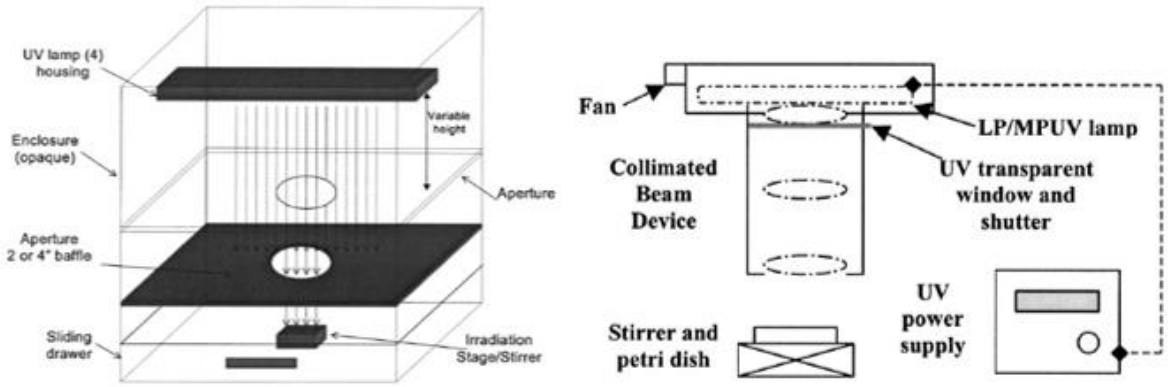

Figure 2.3: Examples of CB apparatus (Bolton and Linden, 2003).

The term UV dose is defined as the integral of UV intensity during the exposure period (USEPA, 2006). For situations in which UV irradiance (or fluence rate) is constant, it is defined as the product of irradiance expressed in milliwatts per square centimeter (mW/cm^2) and the exposure time of the fluid or particle to be irradiated expressed in seconds (s) (Bolton and Linden, 2003).

During UV disinfection, it is crucially essential to accurately determine the UV dose, especially for quantification of photochemical or photobiological kinetic parameters (Qiang et al., 2015). In practical applications, UV dose determination has never been an easy task. For those with uniform UV incident radiation from one direction, the UV dose can be determined following the protocol proposed by Bolton and Linden (2003); in contrast, for those with UV radiation incident from all directions (for example, in an enclosed UV reactor), chemical actinometers can be used to quantify the UV dose (Rahn, 1997).

In whatever application of UV-based technologies, UV radiometers are always a key instrument for irradiance measurements. They are easy to use and have a quick response. However, the radiometer detector sensitivity often declines because of aging; for example, an 18% decrease in 1 year was reported to be a typical value for a detector used at 300 nm (Kuhn et al., 2004). As a result, the radiometer and detector must be calibrated by the radiometer manufacturer at least once per year (USEPA, 2006).

The other well-established approach that can be used to determine UV irradiance is chemical actinometers, with advantages over radiometers such as being able to conform to the reactor geometry and free of periodic calibrations (Jin et al., 2006). A chemical actinometer is a chemical system that undergoes a light-induced reaction with a known quantum yield (Bolton, 2010). Different actinometers in solid, gas and liquid phases have been developed (Kuhn et al., 2004). Among those suitable for UV applications, the KI/KIO_3 actinometer stands out for its operational simplicity and high sensitivity and being free of interference from room light (Rahn, 1997).

2.4 Mechanism of Microorganism Inactivation and Repair

Inactivation of microorganisms by UV radiation is primarily based on the UV-induced photochemical reactions of genetic materials (e.g., DNA) in microorganisms' cells. (Besaratinia et al., 2011). UV-A radiation is inefficient in inducing DNA damages for inactivation due to its low absorption by DNA compared to UV-C and UV-B radiation (Sinha and Hader, 2002). It is also known that the level of pathogen inactivation is affected by the UV intensity delivered to the pathogens and the amount of time the pathogens were exposed to UV radiation. Three major damages contributing to the inactivation of microorganisms are pyrimidine dimers, pyrimidine (6-4) pyrimidone photoproducts, and protein-DNA cross-links (USEPA, 2006).

Microorganisms absorb UV differently, leading to slightly different inactivation responses called the inactivation action spectrum. Figure 2.4 illustrates the action spectra of some microorganisms, along with the relative spectrum of DNA. For bacteria, the maximum response occurs at around 254 nm; however, slightly improved responses for viruses and protozoa have been recorded at higher wavelengths (260–270 nm). The differences in the action spectra probably arise from different compositions of nucleotides in their DNA and RNA (Bolton and Cotton, 2008).

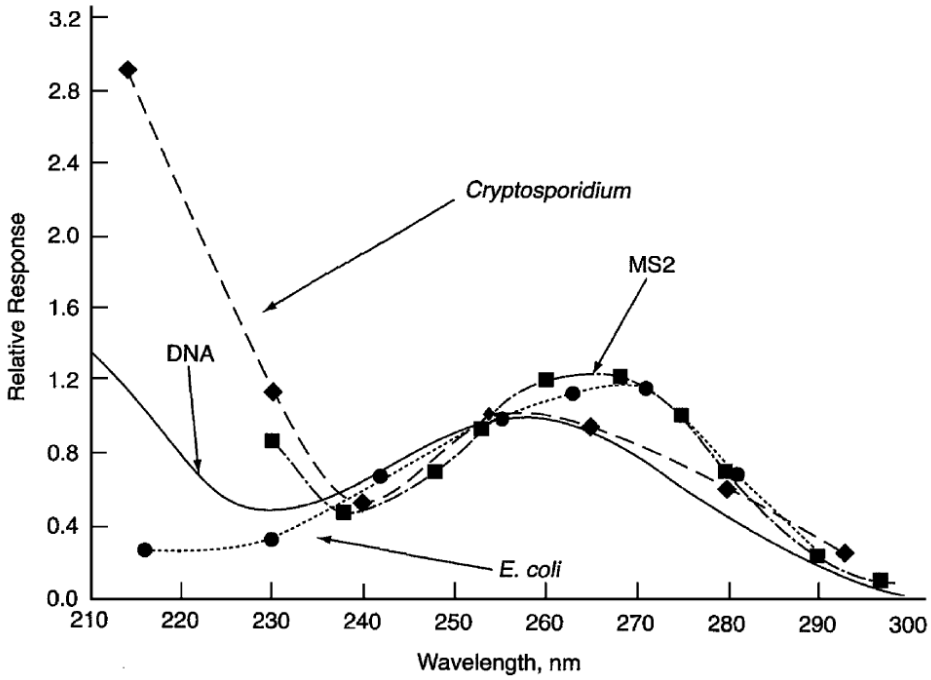

Figure 2.4: Inactivation spectra for *E. coli* (…), MS2 coliphage (-·-), and Cryptosporidium (- -) along with relative spectrum of DNA (—) based on relative response at different wavelengths (Reproduced from Bolton and Cotton, 2008).

Some microorganisms are able to repair the damage caused by UV disinfection through either dark or photoreactivation repair mechanisms (Bolton and Cotton, 2008). DNA repair is a potential drawback of UV disinfection, which is prevalent among various microorganisms such as bacteria (Goosen and Moolenaar, 2008, Hu and Quek, 2008), and the disinfection performance of UV radiation can be deteriorated. For the dark repair mechanism, the microorganism does not require light to repair the DNA damage. However, for photoreactivation mechanism, which is more effective than the dark repair mechanism, UV-A and/or visible light is required to restore the DNA damage (Bolton and Cotton, 2008). Several factors have been reported to affect UV inactivation and repair after inactivation, such as turbidity (Passantino et al., 2004), salinity (Oguma et al., 2013, Rubio et al., 2013), and organic matters (Cantwell et al., 2008, Ou et al., 2011). The indicator bacteria *E. coli* (ATCC 11229) had been reported to be capable of photo-repair following LP UV radiation by several studies (Sommer et al., 2000; Zimmer and Slawson, 2002).

2.5 UV Dose Response and Related Kinetic Model

In order to determine the inactivation of microorganisms as a function of UV dose, a laboratory bench-scale CB apparatus can be used under well-defined laboratory conditions (USEPA, 2006). The results obtained from performing CB tests can be displayed in UV dose-response curves determined by irradiating a sample to UV radiation containing the microorganism with various UV doses and measuring the concentration of microorganisms before and after exposure (Figure 2.5). UV dose-response curves can be expressed as either the proportion of microorganisms inactivated after UV exposure or the proportion of microorganisms remaining as a function of UV dose. UV dose-response curve of microbial inactivation has a positive slope, while microbial survival has a dose-response curve with a negative slope (USEPA, 2006).

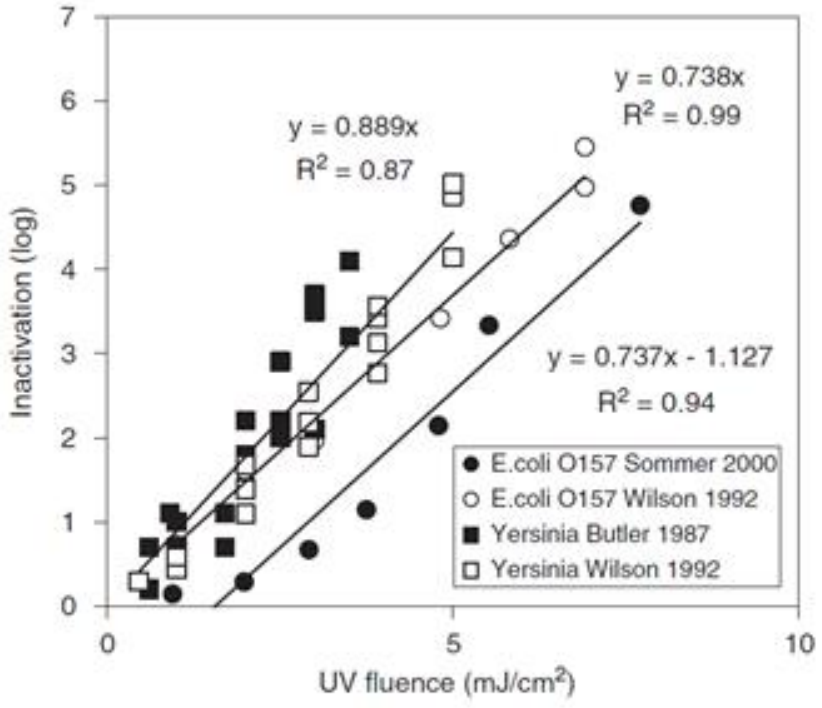

Figure 2.5: UV dose-response curves for pathogenic bacteria (Hijnen, 2006).

The first-order disinfection model of Chick and Watson (1908) is most commonly used to describe the inactivation kinetic for chemical disinfectants. The same model can be applied for UV disinfection. Based on this model, the linear relation between log inactivation and the UV dose is described by:

$$Log\left(\frac{N}{N_0}\right) = -k \cdot D \quad (2.1)$$

Where N_o (CFU/100 mL) is concentration of viable organisms before exposure to UV radiation, N (CFU/100 mL) is concentration of viable organisms after exposure to UV radiation, k (cm^2/mJ) is first-order inactivation rate, and D (mJ/cm^2) is UV dose.

However, under real conditions, this behavior may present shoulder or tailing deviations. Some authors (Knudson, 1985; Hoyer, 1998; Sommer et al., 1998; Mamane-Gravetz and Linden, 2005) observed no inactivation of bacteria or bacterial spores at low UV doses followed by a log-linear kinetic behavior at higher UV doses which can be described as shouldering effect. The second deviation from the linear kinetics is no further increase in inactivation at high doses, called tailing (Hijnen, 2006).

Since the UV dose-response curve is expected to be a characteristic feature of each microorganism species, Malayeri et al. (2016) broadly reviewed literature experimental data for UV inactivation and extracted the UV doses required to achieve defined inactivation extents for bacteria, protozoa, and viruses, as some of them reported in Table 2.1. All data in the table are for microorganisms suspended in water and irradiated with either LP UV light or MP UV light. It can be seen that the UV sensitivity of pathogens differs from one species to the other. Moreover, of the microorganisms of interest in water, bacteria are less resistant to UV inactivation compared to protozoa and viruses.

Table 2.1: UV doses for inactivation of various bacteria, protozoa and viruses (Malayeri et al., 2016).

	UV Dose (mJ/cm^2) for a Given Log Reduction without Photoreactivation							
Bacterium	**Lamp Type**	**1**	**2**	**3**	**4**	**5**	**6**	**Reference**
Enterococcus faecalis ATCC27285	LP	3.7	8	14+ tailing				Moreno-Andrés et al. 2016
E. coli ATCC 11229	LP	2.5	3	3.5	4.5	5	6	Sommer et al. 2001
E. coli ATCC 11229	LP	4.7	6.2	7.2	8.3	9.3	-	Quek and Hu 2008
E. coli ATCC 11229	LP	4.1	5.1	6.2	-	-	-	Bowker et al. 2011
E. coli B ATCC 1303	LP	1.2	3	4.7	6.5	8.2	10	Sholtes et al. 2016

E. coli C3000	LP or MP	3	4.3	5.5	7	-	-	Eischeid and Linden 2000
E. coli K12 IFO 3301	LP	1.9	4	6	8	-	-	Rattanakul et al. 2014
E. coli OP50	LP	2	4.4	6.7	9.1	-	-	Bichai et al. 2009
E. coli O78: H11	LP	4	5	5.5	6	7	-	Sommer et al. 2000
Protozoan								
Acanthamoeba castellan CCAP 1534	LP	32	52	72	-	-	-	Cervero-Arago et al. 2014
Acanthamoeba culbertsoni ATCC 30171	LP	38	58	125	148	-		Maya et al. 2003
Vermamoeba vermiformis 195	LP	10	17	24	32	-	-	Cervero-Arago et al. 2014
Virus								
Adenovirus Type 2; host: A549 cell line	MP	10	20	30	40	50	-	Linden et al. 2007
Adenovirus Type 2 method: LR-qPCR 6kbfragmen; host: A549 cell line (CCL-185)	LP	5	20-50	100	-	-	-	Rodriguez et al. 2013
MS2 coliphage ATCC15977-B1; host: *E. coli* ATCC 15597	LP	18	40	-	-	-	-	Templeton et al. 2006
MS2 coliphage ATCC15977-B1; host: *E. coli* ATCC 15597	LP	20	40	70	95	120	138	Sherchan et al. 2014
Rotavirus SA-11; host: MA 104 cell line	LP	7	15	23	-	-	-	Battigelli et al. 1993
Poliovirus Type 1; host: BGM cell line	LP	8.7	17	25	-	-	-	Shinet al. 2005

2.6 Factors Affecting UV Inactivation

Water quality control prior to UV disinfection processes is of considerable importance to ensure process effectiveness. The ability to inactivate pathogens largely depends on the water quality (Farrell et al., 2018). In particular, the presence of dissolved and suspended matter can significantly affect UV disinfection efficiency through various mechanisms, including scattering and absorption of incident UV radiation and through the shielding of bacteria,

protozoa, and viruses, preventing sufficient UV dose for pathogen inactivation (Huber et al., 2011). In addition to water quality parameters, the potential of pathogens to attach to the surface of particulate matter is an important issue that can affect UV disinfection performance. In the following paragraphs, the most important factors are discussed.

2.6.1 Turbidity

Turbidity is an optical phenomenon induced by the presence of particulate matter in water and wastewater that leads to UV light transmission interference by two major mechanisms that are encasement and shading, as illustrated in Figure 2.6 (Crittenden et al., 2012). Thus, turbidity is one of the parameters that is widely used to measure the quality of water and wastewater prior to disinfection.

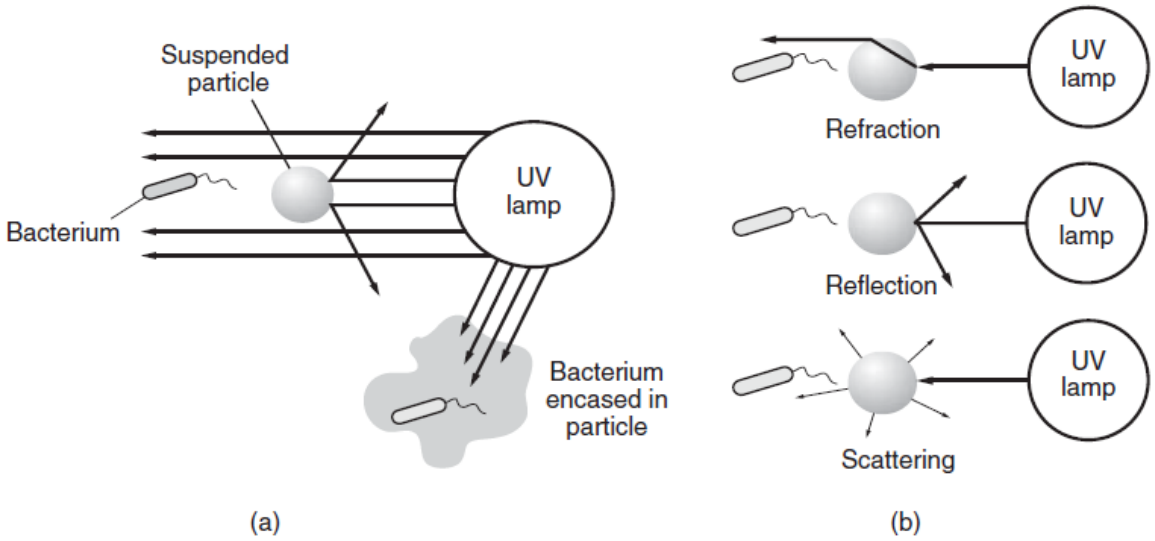

Figure 2.6: Illustration of mechanisms for UV transmission interference by particles: (a) overview of mechanisms for interference and (b) mechanisms of shading (Crittenden et al., 2012).

In Europe and the US, the regulatory requirements for water quality before UV disinfection suggest preserving a level of turbidity lower than 1 NTU (Farrell et al., 2018). The World Health Organization promotes an even lower turbidity threshold of below 0.2 NTU (World Health Organization, 2011). Given the importance of turbidity for UV disinfection, it is essential to understand the effect of different turbidity-causing materials (TCMs) on inactivation using UV radiation.

2.6.2 Absorbance

Absorbance causes the decrease of incident radiation passing through a water sample over a specified distance or path length (Mamane, 2008; USEPA, 2006). UV absorbance at 254 nm (A_{254}) is a water quality parameter commonly used to characterize the DBPs formation potential of water and in general, it is also an indicator of the presence of organic compounds. In UV disinfection applications, according to Equation (2.2), A_{254} is used to measure the amount of UV radiation passing through the water and reaching the target microorganisms, which is called UV transmittance (UVT) (USEPA,2006).

$$UVT = 10^{-A_{254}} \tag{2.2}$$

For measuring A_{254}, a spectrophotometer with 254 nm incident light is used and is typically reported on a per centimeter (cm^{-1}) basis (USEPA, 2006). When UV radiation is absorbed in the water matrix, it is no longer available to disinfect microorganisms. Thus, water with high absorbance can be strongly detrimental to UV disinfection (Mamane, 2008). Several substances in water influence UV absorbance directly, such as iron, nitrate, and natural organic matter. Aquatic natural organic matter has been operationally classified as humic substances and non-humic substances. In turn, humic substances are classified as humic acid, fulvic acid and humin (Mamane, 2008). Sorption of organic matter on colloids or larger particles may impact UV disinfection. In support of this possibility, some studies showed that soil-derived humic acid possibly coated the surface of viruses and bacteria, protecting them from UV (Templeton et al. 2006; Cantwell et al. 2008).

2.6.3 Bacterial Attachment to TCMs

Besides the influence of particles on optical phenomena, another important effect influencing the UV inactivation extent is the potential of microorganisms to attach to the surface of particulate TCMs or be bound together by large organic molecules (Hess-Erga et al., 2008, Liu et al., 2013, Mamane, 2008, Wu et al., 2005). Attachment can add an additional layer of protection to microorganisms due to the proximity to the particulate matter, both by shading and absorbing incident UV radiation, depending on the particulate properties (Farrell et al., 2018).

In Table 2.2, most relevant research works related to the factors affecting UV inactivation are summarized, including a brief description of each study and the obtained results.

Table 2.2: Recent research and their results related to the factors affecting UV inactivation.

Topic, Aim and Description of the Research	Results	Reference
How particles affect UV light in the UV disinfection of unfiltered drinking water ✓ The research was conducted in two phases: • phase 1: particles effect on UV dose transmission • phase 2: impact of particles on the determination of UV absorbance. ✓ Particle size distributions in raw water, taken from the water treatment plant, were prepared by using filters with absolute pore sizes of 5, 11, and 40 μm. ✓ Turbidity range was between 0.1 and 10 NTU. ✓ Both direct and integrating sphere spectrophotometer were used for measuring the absorbance.	1. At a set applied UV dose, an increase of turbidity from 1 to 10 NTU would decrease the average dose from 5 to 33% in the CB test. 2. There were significant differences in UV absorbance coefficients measured using direct and integrating sphere spectroscopy. 3. Using a direct spectrophotometer resulted in underestimating the average UV irradiance by 3 to 20% at turbidity of 3 to 10 NTU, respectively, compared with irradiance calculations made using integrating sphere absorbance measurements. 4. Turbidity greater than 3 NTU led to an overly conservative UV dose determination by the direct absorbance measurement.	Christensen and Linden, 2003
Evaluating water quality effects on UV disinfection of MS2 coliphage ✓ Water quality and sample depth effect on inactivation of MS2 coliphage in 17 filtered waters were evaluated. ✓ The inactivation performance of low-pressure (LP) and medium-pressure (MP) lamp types was compared.	1. The investigated water quality parameters (turbidity, particle count, and size) did not influence the LP and MP disinfection efficiency of seeded MS2 in filtered water at UV doses used in water treatment, while absorbance affected UV dose delivery. 2. UV light from MP lamps appeared more effective than LP UV for inactivating MS2. 3. Results indicated that the inactivation of MS2 coliphage was reduced in the deeper sample.	Batch et al., 2004

Effect of low turbidity and algae on disinfection performance ✓ The research was carried out in two phases of MP UV CB tests: • The first phase compared the dose–response of MS2 bacteriophage in waters with montmorillonite clay turbidity up to 12 NTU and algal content up to 42 µg/L as chlorophyll a (~42,000 cells/mL) to the dose–response of seeded MS2 in deionized water. • The second phase compared phase 1 results with the inactivation of MS2 in natural waters of varying turbidities and algal counts**.**	1. The results of phase 1 indicated that the UV light effectively inactivated MS2 in the presence of turbidity and algal cells typically present in unfiltered drinking water supplies do not negatively affect the ability of UV radiation to inactivate MS2. 2. In phase 2, the inactivation of MS2 in natural waters was statistically different from the inactivation observed in the biological controls. Despite the statistical difference, UV radiation was still effective for inactivating MS2. 3. In phase 2, to achieve a 4-log inactivation, a UV dose of 85 mJ/cm^2 was required whereas in phase 1 the same inactivation required a UV dose of only 70 mJ/cm^2.	Passantino et al., 2004
Impacts of Goethite Particles on UV Disinfection of Drinking Water ✓ The goal of this work was to investigate the UV disinfection performance of drinking water under the impact of freshly generated small sized-goethite particles. ✓ Two microorganisms were employed in this study: *E. coli B* and *Pseudomonas putida*. ✓ Goethite particle concentrations were approximately 0, 1, 5, 10, 20, and 50 mg/L with a turbidity contribution of 0, 1, 5, 10, 20, and 50 NTU, respectively.	1. At the low UV doses, under different turbidity conditions mainly caused by goethite the log reduction values were similar. 2. Goethite particles considerably influenced the UV inactivation efficiency, even at a low concentration of particles with a turbidity range from 1 to 5 NTU. 3. By increasing the attachment time to goethite particles, the log reduction values for both *P. putida* and *E. coli* decreased. 4. The results indicated that small-sized goethite particles protect bacteria from UV disinfection even at very low levels of turbidity (1 to 5 NTU).	Wu et al., 2005
Effect of UV intensity and water turbidity on microbial indicator inactivation ✓ The aim of this study was to investigate the effect of UV intensity and water turbidity on *E. coli*, *Bacillus subtilis*, *Staphylococcus aureus*, *Candida albicans*, and MS-2 coliphage. ✓ 4 cm experimental sample was exposed to UV radiation using the CB apparatus. ✓ Three levels of turbidity (0.5, 4, and 12 NTU) and intensity (0.18, 0.10, and 0.008 mW/cm^2) were selected.	1. High UV disinfection efficiency was obtained by high UV intensity. 2. The results indicated that higher intensity could overcome the negative effect of turbidity under the same UV dose. 3. MS-2 coliphage was not affected by turbidity; however other microorganisms were influenced when turbidity was more than 4 NTU.	Liu and Zhang, 2006

Impact of particle agregated microbes on UV disinfection. II: Proper absorbance measurement for UV fluence ✓ The aim of this research was to evaluate the light scattering effect of particle aggregated microbes on UV disinfection by comparing standard spectrophotometer and integrating sphere absorbance measurements for UV fluence determination. ✓ Two different water types were used in the experiments: (1) a simulated drinking water spiked with spores and clay particles; and (2) natural raw water from the water treatment plant spiked with spores.	1. Measuring the absorbance by using a conventional spectrophotometer in the UV fluence calculation for water with turbidity higher than 3 NTU led to overdosing of the UV system. 2. Using an integrating spectrophotometer could overcome the problem with conventional spectroscopy in absorbance measurements of scattering suspensions. 3. Aggregation protected spores; However, aggregates of natural particles in water protected spores to a greater extent compared to aggregates of added clay particles in simulated waters. 4. Results indicated that particle size could be an important measure to relate to particle–microbe aggregation and related impacts on disinfection.	Mamane et al, 2006
Impact of flocculated particles on low pressure UV inactivation of *E. coli* in drinking water ✓ This study investigated LP UV inactivation of spiked *E. coli* under the effect of coagulated/flocculated particulate matter under drinking water conditions. ✓ Floc particles effects in both coagulated river water and coagulated process (treatment plant) water was evaluated. Laboratory grade water and uncoagulated river water were used as controls. ✓ The turbidity ranges in river water and process water were 12-32 and 5.3-17, respectively.	1. Without coagulation/flocculation, surface water particles with turbidity range from 12 to 32 NTU did not affect UV disinfection if the particles are appropriately accounted for in the UV transmittance determination. 2. Forming of floc particles in the presence of coagulation and flocculation resulted in less inactivation of *E. coli*. 3. Results indicated that particle size data could be of great value in addition to turbidity in setting criteria for UV disinfection processes.	Liu et al., 2007
Inactivation of particle-associated viruses by UV ✓ The aim of this research was to investigate the behavior of disinfecting particle-associated viruses via UV radiation. ✓ Various waters (tap water, reservoir water, and secondary effluent) were used in this study. ✓ Turbidity for tap water, reservoir water, and secondary effluent were 0.3, 4.2 and 2.1, respectively. ✓ Particle size ranges (μm) were: • Tap water: 0.0464– 0.073 • Reservoir water: 38.3– 222.4 • Secondary effluent: 2.8– 179.2	1. A two-stage survival phenomenon was observed for UV disinfection of bacteriophage MS2 in different waters containing particles: • the first stage represented a rapid inactivation which corresponds to dispersed virus inactivation. • the second one represented a slow inactivation which corresponds to particle-associated virus inactivation. 2. The presence of turbidity and coliform bacteria adversely influenced the UV disinfection efficiency. 3. The efficiency of UV disinfection was affected by particle size, number of particles, and particle size distribution.	Hu et al., 2007

Inactivation of indigenous coliform bacteria in unfiltered surface water by ultraviolet light ✓ This study investigated the potential for naturally occurring particles to protect indigenous coliform from UV disinfection in four unfiltered surface waters, all with an indigenous total coliform count of 100 CFU/100mL or greater. ✓ The turbidity ranged from 0.79 to 2.9NTU and TOC from 2.6 to 7.3 mg/L. The UV transmittance at 254 nm ranged from 60 to 96% (expressed per cm). ✓ A spectrophotometer equipped with a fixed integrating sphere accessory was used to measure the UV transmittance of the water.	1. Tailing in the UV dose-response curve of the bacteria was observed, implying particle-related protection. 2. By comparing coliform UV inactivation data for parallel filtered (11 mm pore-size nylon filters) and unfiltered surface water, the effect of particles was confirmed. 3. Results indicated that particles as small as 11 mm, naturally found in surface water with low turbidity (<3 NTU), are able to harbor indigenous coliform bacteria and offer protection from low-pressure UV light.	Cantwell and Hofmann, 2008
Effect of particles and bioflocculation on ultraviolet disinfection of *Escherichia coli* ✓ The goal of this research was to investigate the UV disinfection performance under the effect of particles and flocs by using a synthetic system that can simulate the bioflocculation of particles and microorganisms in water and wastewater samples. ✓ *E. coli*, latex particles (1, 3.2, 11, 25, and 45 μm), alginate, and divalent cations were used for the synthetic system, and the bioflocculation of particles was achieved naturally as it would occur in the environment.	1. At UV doses lower than 9 mJ/cm^2, particle size and degree of flocculation did significantly impact on the *E. coli* inactivation. 2. Only at high UV doses and for larger particles and well-flocculated samples, the effect of particles and bioflocculation on *E. coli* inactivation was statistically significant. 3. According to the results, even without particles, some of the self-aggregated *E. coli* could survive a UV dose of 90 mJ/cm^2. Association of *E. coli* with particles and flocs, however, provided a higher level of protection and resulted in lower inactivation levels for the particle sizes tested. 4. Many factors related to microbe, particle, and solution characteristics, as well as the size of particles and flocs, are important in determining the overall efficiency UV disinfection efficiency.	Kollu and Ormeci, 2012

Turbidity composition and the relationship with microbial attachment and UV inactivation efficacy ✓ In this research, the characteristics and bacterial attachment to TCMs were evaluated and the resultant effect on UV disinfection was determined. ✓ Fe (III) hydroxide precipitate, chalk, kaolin clay, manganese dioxide, and humic acids were considered as TCMs at different turbidity levels ranging from 0 to 5 NTU. ✓ *E. coli* (ATCC 25922) and *E. faecalis* (ATCC 29212) were used to perform the experiments. ✓ The UV inactivation experiments were carried out using a UVC-LED system.	1. Humic acids and Fe(III) had the most influence on *E. coli* and *E. faecalis* inactivation because of decreasing UV transmittance with increasing the concentration of TCM. 2. *E. coli* and *E. faecalis* attachment was only seen for chalk and Fe(III). The attachment was assumed to be as a result of these particles having a more neutral surface charge. 3. The presence of some TCMs substantially lowered the *E. coli* inactivation for Fe(III) and humic acids, with some of this attributed to attachment, but the majority due to reductions in UVT. 4. *E. faecalis* was more resistant to UV inactivation in the presence of TCMs than *E. coli.*	Farrell et al., 2018

Table 2.2 indicated that many studies had been broadly examined UV inactivation under the impact of dissolved and suspended matters, affecting UV disinfection performance. The results of past studies showed the importance of turbidity and absorbance throughout the experiments that their effect should be considered precisely for water and wastewater systems in order to enhance UV disinfection efficiency. However, further studies are needed to investigate the sufficiency of correction factors that are applied to obtain the estimated delivered UV doses to microorganisms in different sample depths with different optical properties.

CHAPTER 3. MATERIALS AND METHODS

This present chapter is structured in three sections, including the UV inactivation experiments using CB apparatus (Section 3.1), UV disinfection modeling for CB apparatus and UV disinfection reactor (Section 3.2), and materials used in this study (Section 3.3).

3.1 UV Inactivation Experiments

3.1.1 Experimental Design

Full-Factorial design is the statistical technique used in this study for the design of experiments (DoE), where two factors are controlled, and their effects are investigated at each of three levels (Dieter and Schmmidt, 2009). The experimental design was defined in order to investigate the impact of turbidity and absorbance on UV dose reduction at three different sample depths of 1, 2.5, and 4 cm. In this case, turbidity and absorbance were chosen as DoE factors. The compounds selected as models for turbidity and absorbance were kaolinite and humic acid, respectively. Nine experimental conditions were tested for 4 cm sample depth, combining different optical characteristics of the water matrix in terms of turbidity (0-10 NTU) and absorbance (0-0.2 cm^{-1}). Turbidity and absorbance were obtained by diluting kaolinite and humic acid in deionized water (DI), respectively. In addition, for samples with 1 and 2.5 cm depth, a reduced experimental design was carried out, limiting tests to pure water matrix and highest concentrations of kaolinite and humic acid. For each experimental condition, inactivation experiments were conducted in triplicates. Table 3.1 and Figure 3.1 represents the experimental design.

Table 3.1: Experimental Design: identifying the three levels (-1, 0, +1) of each factor (turbidity and absorbance) for three different sample depths.

		Factor Levels		Factors	
	Experiment #	**Turbidity**	**Absorbance**	**Turbidity (NTU)**	**Absorbance (cm^{-1})**
4 cm Sample Depth	1	-1	-1	0	0
	2	-1	0	0	0.1
	3	-1	1	0	0.2
	4	0	-1	5	0
	5	0	0	5	0.1
	6	0	1	5	0.2
	7	1	-1	10	0
	8	1	0	10	0.1
	9	1	1	10	0.2

2.5 cm sample path length	**1**	**-1**	**-1**	**0**	**0**
	9	1	1	10	0.2
1 cm sample path length	1	-1	-1	0	0
	9	1	1	10	0.2

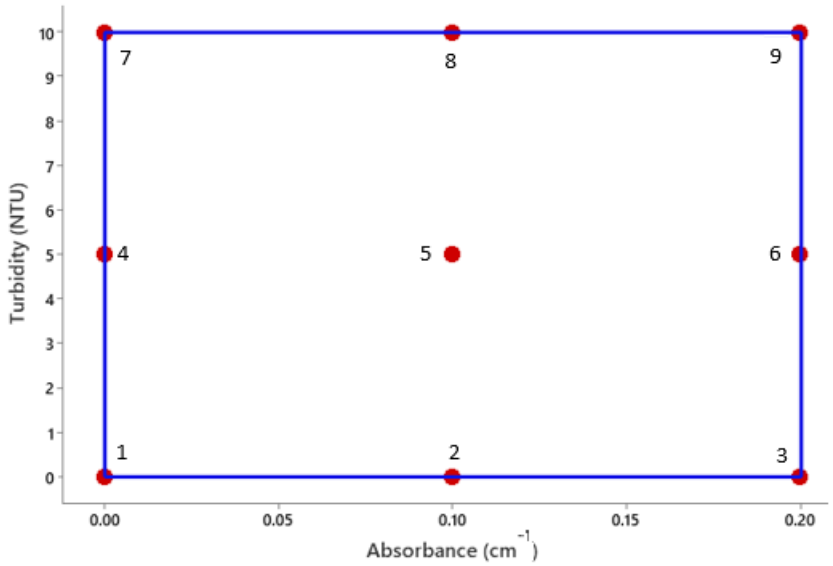

Figure 3.1: Experimental design representation: full-factorial design with two factors (turbidity and absorbance) and 3 levels each (-1, 0, +1).

3.1.2 Water Matrix Characterization

Water matrices were characterized by measuring turbidity and absorbance at a wavelength of 254 nm. To prepare synthetic water samples with different turbidity levels, kaolinite was measured using a Kaolinite - Turbidity standard curve (Figure 3.2), which was defined by plotting kaolinite concentration (mg/L) against turbidity (NTU). In this case, five sample tests of kaolinite solutions with a value range of 2.5-25 mg/L were chosen, and the turbidity of each sample was measured by a TB1 portable turbidimeter (Velp Scientifica) calibrated according to the manufacturer's instructions (Table 3.2).

Table 3.2: The average turbidity measurements used for determining the Kaolinite – Turbidity standard curve.

Sample	Kaolinite Concentration (mg/L)	Turbidity (NTU)
1	2.5	2.54
2	5	4.85
3	10	8.99
4	12.5	10.48
5	25	21.36

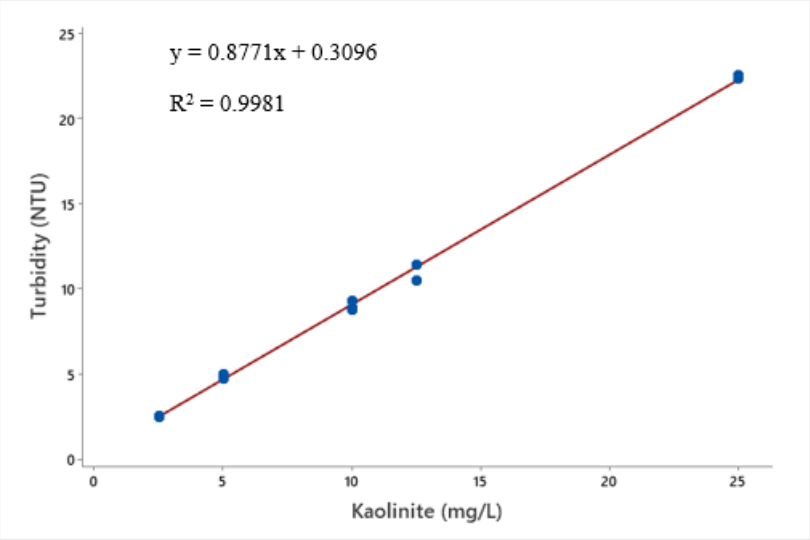

Figure 3.2: Kaolinite – Turbidity standard curve applied for the estimation of the kaolinite concentration of water matrices given the turbidity measurement.

Similarly, by using five humic acid solutions ranging from 2.5 to 25 mg/L, a Humic acid - Absorbance standard curve at the wavelength of 254 nm was determined to estimate the concentration of humic acid in the water matrices as a function of a given absorbance value. In Table 3.3 and Figure 3.3, the average absorbance measurements for different humic acid concentrations and related standard curve are presented, respectively. The absorbance values of samples were measured with a DR6000 spectrophotometer (Hach). In this case, rectangular quartz cuvettes with a 1 cm path length were used.

Table 3.3: The average absorbance measurements used for determining the Humic acid – Absorbance standard curve.

Sample	Humic Acid Concentration (mg/L)	Absorbance (cm^{-1})
1	2.5	0.076
2	5	0133
3	10	0.268
4	12.5	0.333
5	25	0.659

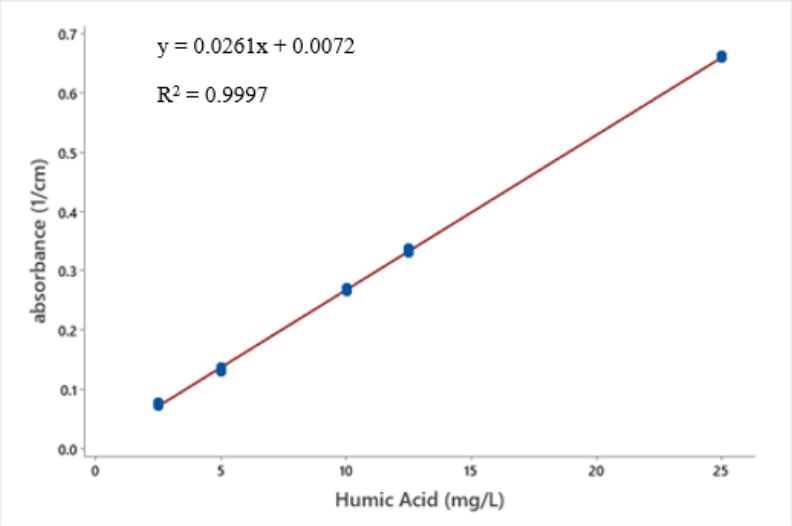

Figure 3.3: Humic acid – Absorbance standard curve applied for the estimation of the humic acid concentration of water matrices given the absorbance measurement.

3.1.3 *E. coli* Pure Culture Preparation and Cell Enumeration

The culture preparation method applied in this study followed the methodology described by Henao et al. (2018). Experiments were performed with a pure culture of microbial indicator organism *E. coli* (DH5α) provided by the Laboratory of Environmental Engineering of Politecnico di Milano (LIA). The liquid broth (LB) (10 g/L of tryptone, 5 g/L of yeast extract, and 5 g/L of NaCl) and the saline solution (9 g/L of NaCl) for bacteria cultivation were prepared in DI water and sterilized in the autoclave at 120 °C for 20 minutes. To cultivate *E. coli*, a bacterial colony was collected with a sterile inoculating loop from the stock agar Petri dish and suspended in a sterile Falcon tube containing approximately 25 mL sterile LB. The same procedure was repeated for three tubes, while a parallel control tube was prepared. Then, bacterial cultures were incubated at 37°C for 18-24 hours in the incubator (M60-TB, MPM Instruments) with continuous mixing speed at 90 rpm to stimulate the bacteria to grow under exponential conditions. After the incubation period, samples were centrifuged for 20 min at 4000 rpm. The supernatant was removed and discarded, while *E. coli* pellets were resuspended in 25 mL of sterile saline solution to achieve a cell count of approximately 10^8 to 10^9 CFU/mL. For cell enumeration, the membrane filtration method was used to estimate bacterial concentration in samples. A sterile membrane for microbiology with 0.45 μm pores and 47 mm diameter was used for filtration of each sample to retain the microorganism. The viable cells were enumerated by placing the membrane on a Petri dish with chromogenic substrate C-EC Agar (Biolife) and incubating at 37 °C for 18–24 h.

3.1.4 Chemical Actinometry

The iodide/iodate (KI/KIO_3) actinometer based on the protocol for the irradiance measurement from the LP UV lamp described by Bolton et al. (2011) was used.

The actinometer solution does not absorb light above 320 nm, so it can be used safely in room light. The overall photochemical reaction is:

$$8I^- + IO_3^- + 3\ H_2O + h\nu \longrightarrow 3\ I_3^- + 6\ OH^- \quad (3.1)$$

For performing the actinometry test, 100 mL of the KI/KIO_3 actinometer stock solution was prepared, consisting of 0.60 M KI, 0.10 M KIO_3, and 0.01 M sodium tetraborate ($Na_2B_4O_7 \cdot 10H_2O$). It should be noted that the solution was used within 4 hours after preparation due to the very slow thermal reaction between iodide and iodate. After preparation of the actinometer solution, the test was performed as follows:

- 5 mL of the actinometer solution was mixed by magnetic stirrer using a stir bar for 8 minutes and the absorbance of unirradiated actinometer solution at a wavelength of 352 nm was measured (A_{blank_1}).
- Then, another 5 mL of the actinometer solution was mixed by magnetic stirrer using a stir bar in a 20 mL beaker covered by a washer with a hole with a cross-sectional area of 1.327 cm^2 and exposed to UV radiation for 8 minutes. The absorbance at 352 nm was measured (A_{Sample}).
- After the UV exposure, the absorbance of an unirradiated actinometer solution at 352 nm was measured again (A_{blank_2}).
- The temperature of the actinometer solution before and after the UV radiation was measured and the average temperature was calculated.

Subsequently, according to the following equations, the quantum yield Ø (-), triiodide ion moles formed m (moles), and UV incident irradiance E (mW/cm^2) that was corrected for 2.5% of water surface reflection were estimated.

$$\emptyset = 0.71 + 0.0099(T - 24) \quad (3.2)$$

$$m = \frac{A(sample)_{352} - A(blank)_{352}}{\varepsilon} \times V \quad (3.3)$$

$$E = \frac{m}{(A \times t) \times \emptyset} \times 471420.89\ (J\ einsteins^{-1}) \times \frac{1}{0.975} \qquad (3.4)$$

Where T (°C) is the average temperature of the solution, A(sample) (-) is the absorbance of irradiated actinometer solution at 352 nm, $A(blank)_{352}$ (-) is the average absorbance of unirradiated actinometer solution before and after UV irradiation at 352 nm (average of $A_{(blank\_1)}$ and $A_{(bkank\_2)}$), ε (M^{-1} cm^{-1}) is the molar absorption coefficient, V (L) is the volume of actinometer solution, A (cm^2) is the cross-sectional area of the washer, and t (seconds) is the exposure time of UV radiation.

3.1.5 Collimated Beam Apparatus

A standard bench-scale CB apparatus was built according to the guidelines proposed by Bolton and Linden (2003) for the evaluation of inactivation of a specific microbial population. The CB apparatus (Figure 3.4) equipped with a 30-W LP mercury lamp placed in the center of an enclosed horizontal tube with 12 cm in diameter, a ventilation system, a shutter to block or allow the passage of UV light, and a collimating tube with the length of 54 cm and a diameter of 6 cm to provide spatially homogeneous radiation on the samples with standardized parallel rays of germicidal light. Lamp radiation wavelength was 253.7 nm. The lift platform for holding the Petri dish and the magnetic stirrer was adjusted to have a 1 cm distance from the end of the collimating tube to the surface of the sample in the petri dish.

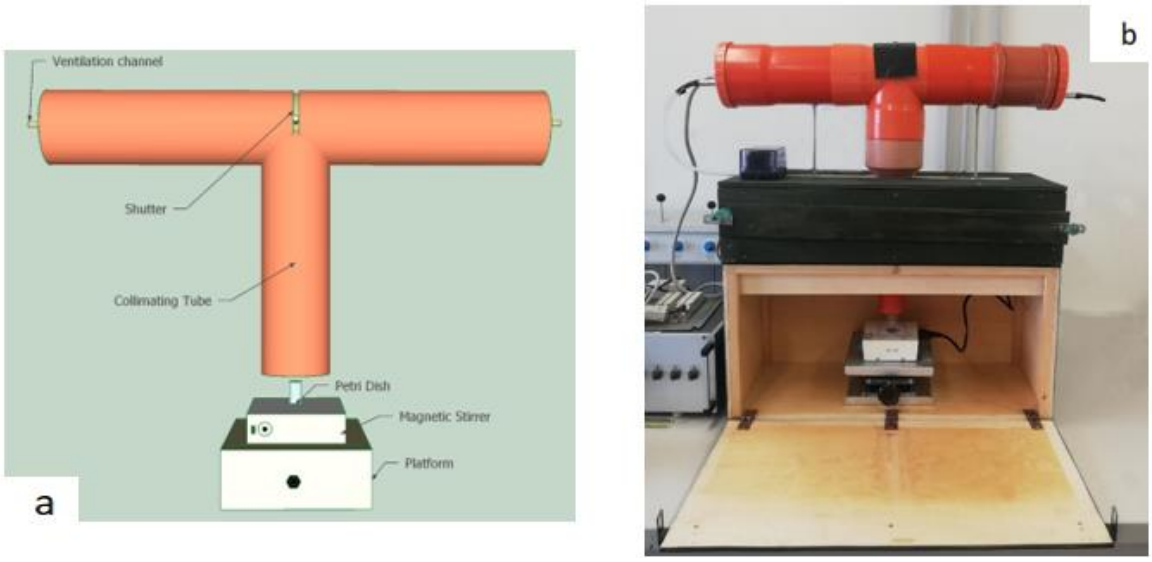

Figure 3.4: CB apparatus used for experiments: (a) schematic figure and (b) picture of the built CB apparatus.

3.1.6 Experimental Protocol for UV Inactivation Experiments

Samples were prepared and spiked with *E. coli* to an initial concentration of approximately 10^6–10^7 CFU/mL in the view of having a concentration sufficient for achieving at least 5-log inactivation. To compare UV dose-response curves of *E. coli* inactivation at different sample depths, samples were exposed in 1, 2.5, and 4 cm deep volumes in 20 mL beakers with a diameter of 2.6 cm. The UV lamp was turned on 30 minutes before starting the experiment for allowing the lamp to warm up and reaching stable radiation intensity. Then, samples were exposed to UV radiation from the LP lamp. Irradiation vessels were placed on top of a magnetic stirrer and continuously mixed with a stir bar while undergoing radiation. The stirring rate was carefully set so that there was no vortex forming on the sample surface. A laboratory lift platform was used to adjust the sample height to provide the same irradiance at the sample surface. Typical germicidal irradiance at the surface of the samples, which was measured by a radiometer (ILT 1400, International Light) and calculated by chemical actinometry test described in section 3.2, was 0.126 mW/cm^2. Samples were exposed to different UV doses for LP exposures provided in Tables 3.4, 3.5, and 3.6. After selecting the target UV dose, sampling times were determined according to Equation 3.5:

$$D = t \cdot E_0 \tag{3.5}$$

Where D (mJ/cm^2) is UV dose, t (s) is the exposure time, and E_0 (mW/cm^2) is the UV irradiance of the LP lamp at the center of the sample surface.

Table 3.4: The applied UV doses (mJ/cm^2) without any correction and the corresponding exposure times at which samples were irradiated for 4 cm sample depth.

Pure water matrix and samples only containing different kaolinite concentration (5-10 NTU)		**Samples containing different kaolinite concentration (5-10 NTU) with 3.5 mg/L of humic acid**		**Samples containing different kaolinite concentration (5-10 NTU) with 7 mg/L of humic acid**	
UV Fluence (mJ/cm^2)	**t (s)**	**UV Fluence (mJ/cm^2)**	**t (s)**	**UV Fluence (mJ/cm^2)**	**t (s)**
3.8	30	6	48	8	63
5.6	45	9	72	12	95
7.6	60	12	96	16	127
9.5	75	15	120	20	159
11.3	90	18	144	24	191

Table 3.5: The applied UV doses (mJ/cm^2) without any correction and the corresponding exposure times at which samples were irradiated for 2.5 cm sample depth.

Pure water matrix (with no kaolinite and humic acid)		**Samples containing 10 mg/L of kaolinite with 7 mg/L of humic acid**	
UV Fluence (mJ/cm^2)	**t (s)**	**UV Fluence (mJ/cm^2)**	**t (s)**
3.8	30	6.4	50
5.6	45	9.4	75
7.6	60	12.6	100
9.5	75	15.6	125
11.3	90	18.7	150

Table 3.6: The applied UV doses (mJ/cm^2) without any correction and the corresponding exposure times at which samples were irradiated for 1 cm sample depth.

Pure water matrix (with no kaolinite and humic acid)		**Samples containing 10 mg/L of kaolinite with 7 mg/L of humic acid**	
UV Fluence (mJ/cm^2)	**t (s)**	**UV Fluence (mJ/cm^2)**	**t (s)**
3.8	30	4.5	36
5.6	44	6.7	53
7.3	58	8.9	71
9	72	11.1	88
10.8	86	13.3	105

After turning on the lamp for 30 minutes to reach the stable condition, the shutter was opened for a required time to irradiate the sample for a given UV dose, and then as the shutter closed, a certain amount of volume was sub-sampled, after that by opening the shutter, the remained sample was exposed to another UV dose and the procedure was repeated. It should be mention that the sampled volume was determined not to exceed 10 percent of the total sample volume. Then, inactivation was measured by comparing *E. coli* survival concentration (N) at a given dose with the *E. coli* starting concentration (N_0). The log inactivation at each dose was calculated as Log10 (N_0/N).

3.1.7 Average Germicidal Irradiance Calculation Throughout the Sample

For determining the average germicidal irradiance throughout the sample, several practical correction factors have been identified by Bolton and Linden (2003). These factors include reflection factor, Petri factor, water factor, and divergence factor.

The reflection factor accounts for the reflection of UV light at the air-water interface. For a normal incident light, the fraction of light reflected is given by the Fresnel law. Based on the Fresnel law and the types of media (air and water), the reflection factor for the CB apparatus was 0.975, and it represents the portion of the light entering the test sample (Bolton & Linden, 2003).

Petri factor is defined as the ratio of the average intensity across the sample surface to the intensity measured at the center of the sample surface (Bolton & Linden, 2003). To determine the Petri factor, UV intensity at the center of the UV beam and every 0.5 cm in the x and y directions for a distance of 2.6 cm were measured using a radiometer (Figure 3.5). Then, these measurements were divided by the irradiance at the center and finally, an average of these ratios were taken. The calculated Petri factor in this study was 0.9008.

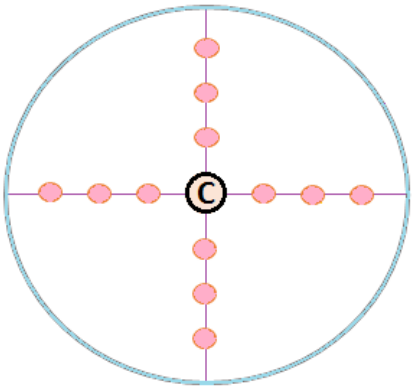

Figure 3.5: The schematic of the points in the area of the Petri dish at which the irradiance of the UV lamp was measured by the radiometer.

The water factor is related to the absorption of UV light by the sample and the sample depth. It was calculated according to Equation 3.6.

$$F_W = \frac{1 - 10^{-Al}}{A \cdot l \cdot ln(10)} \tag{3.6}$$

Where F_w is the water factor, A is the absorption coefficient (cm^{-1}) and l is the vertical path length of the sample (cm).

The divergence factor accounts for the divergence of UV light as it travels from the lamp to the surface of the sample and through the sample (USEPA, 2006), and it was calculated according to Equation 3.7.

$$F_D = \frac{L}{L + l} \tag{3.7}$$

Where F_D (-) is the divergence factor, L (cm) is the distance between UV lamp and sample surface and l (cm) is the sample depth.

Finally, the average germicidal fluence rate E_{ave} (mW/cm^2) was obtained according to the following Equation 3.8.

$$E_{ave} = E_0 . F_R . F_P . F_W . F_D \tag{3.8}$$

Where E_0 (mW/cm^2) is the UV irradiance at the center of the dish.

3.1.8 Data Analysis

Data analysis for experimental results of UV inactivation tests in the CB apparatus was conducted with the statistical software Minitab (release 19). For all experimental conditions defined in the DoE, a linear regression analysis was performed between the applied UV dose and log inactivation of *E. coli*, obtaining a UV inactivation rate constant for each of the experiments. In the next step, a general linear model (GLM) was used to determine the impact of turbidity and absorbance on UV inactivation rate constant. In this case, a complete GLM with Equation 3.10 was defined considering both single variable and variable interaction terms up to the second order and then this complete GLM was simplified in equation 3.11 by considering only single variable and variable interaction terms up to the first order, defining the obtained UV inactivation rate constants as response variables and the measured absorbance and turbidity levels as independent variables:

$$Y = \beta_0 \sum_{j=1}^{k-1} \beta_j X_j + \varepsilon \quad (3.9)$$

$$Y = \beta_0 + \beta_1 X_1 + \beta_2 X_2 + \beta_3 X_1^2 + \beta_4 X_2^2 + \beta_5 X_1 X_2 + \varepsilon \quad (3.10)$$

$$Y = \beta_0 + \beta_1 X_1 + \beta_2 X_2 + \beta_3 X_1 X_2 + \varepsilon \quad (3.11)$$

Where Y is the dependent variable or response variable, Xj is the independent variable, (k-1) is the number of independent variables, βj is the regression coefficients, and ε is the random error.

3.2 UV Disinfection Modeling

The CFD software used in this work for modeling CB apparatus and UV reactor was the commercial software Ansys Fluent (version 2020 R2). CFD generally needs the flow domain to be divided into a grid or mesh. This is essentially a discrete representation of the domain with a number of small volumes, which permits the relevant equations to be solved numerically. In this study, the geometry and computational meshes were produced using GAMBIT 2.4.6 software (Fluent Inc). Several computational meshes were evaluated, including both fine and coarse and structured and unstructured hexahedral meshes. In the following sections the modeling setup for both CB apparatus and UV reactor are described.

3.2.1 CB Apparatus Modeling Setup

For CB apparatus, to obtain the precise average germicidal irradiance and propagation of UV radiation throughout the sample, a 3D geometry model with hexahedral and tetrahedral meshes was constructed. The meshes are composed of an adequate high number of finite elements (approximately 1 million) to ensure an accurate computational solution. As the discrete ordinate (DO) model has emerged as a good choice for the solution of Radiative Transfer Equation (RTE), especially for UV disinfection (Ho, 2009), this model was used for simulating the fluence rate distribution in CB apparatus. The DO model solved RTE for a finite number of discrete solid angles, defined by appropriately setting the parameters for angular discretization, in which the value of 10 was chosen for all. Moreover, non-gray radiation with a wavelength between 253 and 255 nm was considered as the germicidal radiation output of the UV lamp. A semi-transparent boundary condition type was chosen for the water surface and inlet radiation boundary, applying direct irradiation, which was calibrated according to the

measured UV irradiance on the center of the sample surface by the radiometer, while an opaque boundary condition type was set for other walls with an internal emissivity and diffuse fraction equal to one.

For describing the distribution of radiation in the sample, the optical properties of different kaolinite concentration ranging from 6.5 to 50 mg/L, such as absorption coefficient (k), scattering coefficient (σ), extinction coefficient (β), and asymmetry factor (g) were calculated using the spectrophotometer measurements for the wavelength of 254 nm by solving the RTE utilizing the DO method. These calculations were made in the previous study by Baldasso (2020), and the results (Table 3.7) were used to simulate CB apparatus and UV disinfection reactor in this study.

Table 3.7: Optical properties of kaolinite suspensions at wavelength of 254 nm (Baldasso, 2020).

σ (cm^2/mg)	**k (cm^2/mg)**	**β (cm^2/mg)**	**g (cm^2/mg)**
5.86	0	5.86	0.665

For optical properties, a constant absorption coefficient was assigned to water matrices, while the scattering coefficient was calculated by a user-defined function (Table 3.8). The refractive index of water was considered equal to 1.372 (Baldasso, 2020).

Table 3.8: Optical properties assigned for water matrices in CB apparatus.

	Experiment #	**Scattering coefficient (m^{-1})**	**Absorption coefficient (m^{-1})**
4 cm sample depth	1	0	0.43
	2	0	4.41
	3	0	8.38
	4	1.29	0.43
	5	1.29	4.41
	6	1.29	8.38
	7	2.59	0.43
	8	2.59	4.41
	9	2.59	8.38
2.5 cm sample depth	1	0	0.43
	9	2.59	8.34
1 cm sample depth	1	0	0.43
	9	2.59	8.34

3.2.2 UV Disinfection Reactor Modeling Setup

The UV disinfection reactor was modeled according to the same operating conditions as discussed by Baldasso (2020). In this case, experiments #1, #2, #4, and #5 as defined in Table 3.1, were simulated for the flowrates of 1.5, 3, and 5.2 L/min. In addition, two field household water treatment prototypes installed in Mexico for two different raw water sources were modeled with a flowrate of 3.3 L/min. In order to validate the modeling, field data from prototypes installed in Mexico were used (Baldasso, 2020).

Firstly, 3D structural hexahedral meshes with a top-down approach using the multi-axis Cooper algorithm were generated for the domain of the reactor. The domain was discretized to sufficiently refined mesh to guarantee the accuracy of results, which had a total number of 1.39 million finite elements. Then, a no-slip condition was set for the boundary conditions of reactor walls, UV lamp, and quartz tube. The inlet boundary condition was set to velocity inlet with a parabolic velocity profile magnitude, and the outlet boundary conditions were set to pressure outlet. Both inlet and outlet turbulence conditions were defined with a 5% of turbulent intensity over the hydraulic diameter. The realizable k-ε model was employed for the hydrodynamics modeling, which is a model that satisfies certain mathematical constraints on the Reynold stresses consistent with the physics of turbulent flows. Numerical convergence was defined at scaled residuals smaller than 10^{-5} for second-order upwind solutions.

The fluence rate distribution was modeled like the one discussed for the CB apparatus, defining by appropriate parameters for angular discretization (value of 8 was chosen for all). Also, the wavelength interval for non-gray radiation in the reactor chamber for the germicidal radiation output of the UV lamp was as the same range considered in the CB apparatus modeling. The optical properties, including constant absorption, scattering coefficients, and refractive indices for the water matrices in experiments #1, #2, #4, and #5 were specifically set equal to the values used for CB apparatus modeling (section 3.2.1). In Table 3.9, these values for two different water sources used in prototypes in Mexico are provided. The UV lamp surface was set as semi-transparent with a diffuse irradiance of 276 W/m^{-2}, calculated as the ratio between the lamp's UVC output which was 25% of the UV lamp's power (Philips Lighting, 2019), and the UV lamp's surface. The quartz sleeve's inner and outer surfaces were set as semi-transparent with a diffuse fraction of 0, and the external reactor surfaces were set as opaque with reflectivity of 0.26 and a diffuse fraction of 0.1 (Li et al., 2017).

Table 3.9: Absorption coefficient, scattering coefficient, and refractive index for two different water matrices tested.

Element	Scattering Coefficient (m^{-1})	Absorption Coefficient (m^{-1})	Refractive Index (-)
Water Hole	2.26	6.99	1.372
Water Spring	0	3.22	1.372

For the discrete phase model, the microorganisms were injected at the inlet by defining an injection through the Lagrangian particle tracking function. First, a massless surface injection of particles representing microorganisms was defined. Then the particle tracking was computed through the discrete random walk model, considering 10 particles injected for each inlet surface cell. In addition, by implementing a user-defined function, the cumulative dose (J/m^2) was calculated as the product of the irradiance (W/m^2) and the exposure time (s) at each step length of the particle path.

The predicted log inactivation values were calculated using UV doses obtained from CFD simulation and the microorganism inactivation rate constant determined through the inactivation experiments with the CB apparatus.

Figure 3.6 shows the overall CFD process modeling for both CB apparatus and UV reactor.

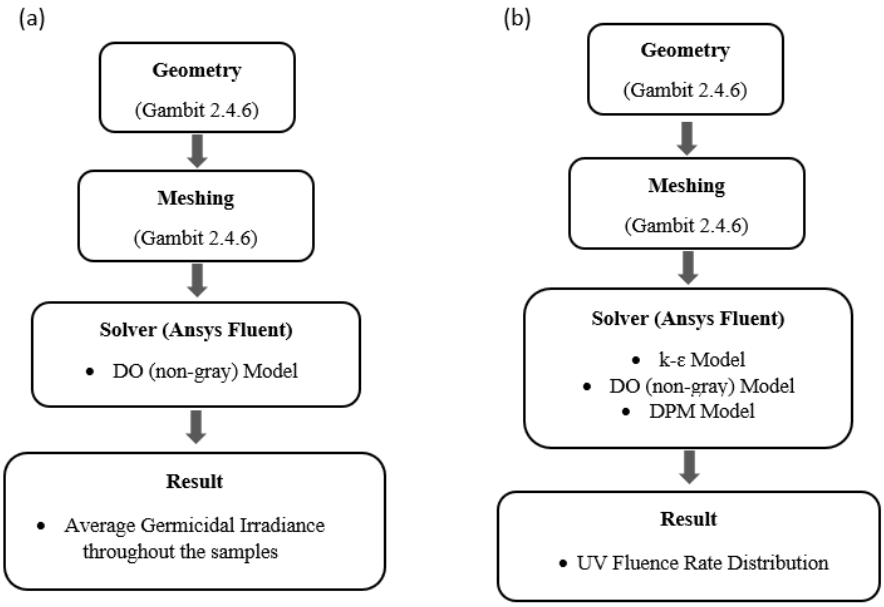

Figure 3.6: Schematic flow chart of simulations for (a) CB apparatus and (b) UV disinfection reactor.

3.3 Materials

All the chemical compounds utilized for the experiments in this study are summarized in Table 3.10.

Table 3.10: Chemical compounds used for the laboratory experiments.

Compound	Product Code	Provider
Kaolinite	03584	Sigma- Aldrich
Humic Acid Sodium Salt	H16752	Sigma- Aldrich
Potassium Iodate	26840.235	VWR
Potassium Iodide	131542.1209	PanReac AppliChem
Sodium tetra-Borate	131644	PanReac AppliChem
Deionized Water	-	Laboratory of Environmental Engineering of Politecnico di Milano (LIA)
E. coli (DH5α)	-	Laboratory of Environmental Engineering of the Politecnico di Milano (LIA)

CHAPTER 4. RESULTS AND DISCUSSION

The main experimental and modeling results are described in this chapter. In section 4.1, the results of UV inactivation experiments are discussed, while in section 4.2, the modeling results for CB apparatus and UV disinfection reactor are addressed.

4.1 UV Inactivation Experiments

4.1.1 Water Matrix Characterization

The primary purpose of conducting the experiments using CB apparatus in this work was to evaluate the inactivation of *E. coli* by UV radiation under different optical conditions of the water matrix, characterized by the presence of kaolinite and humic acid accounting for turbidity and absorbance, respectively. To this end, the measured properties of water matrices are reported in Table 4.1, and it should be mentioned that due to the difficulty of preparing homogenous synthetic samples for obtaining accurate measurements, there are slight differences in the measured values for turbidity and absorbance as compared to those defined in the experimental design.

Table 4.1: Measured properties of water matrices.

Experiment	Turbidity (NTU)	Absorbance (-)
1	0	0.002
2	0	0.100
3	0	0.190
4	5	0.003
5	4.92	0.103
6	5.12	0.193
7	9.86	0.003
8	9.73	0.118
9	10.07	0.203
1	0	0.004
9	9.89	0.208
1	0	0.005
9	10.11	0.200

It should be noted that for the present research, absorbance was measured by direct spectrophotometer, and as the turbidity ranged from 0 to 10 NTU in the water samples, absorbance measurements were likely overestimated due to non-differentiation between

absorbance and scattering. Thus, integrating sphere spectrophotometer would be necessary to improve the absorbance measurements as discussed by Christen and Linden (2003) and Mamane et al. (2006).

4.1.2 Inactivation of *E. coli* Using Collimated Beam Apparatus

The log inactivation results of three replicates of each experimental condition for sample depths of 4, 2.5, and 1 cm are illustrated in Figures 4.1, 4.2, and 4.3, respectively. In these graphs, the y-axis represents the log of *E. coli* concentration before exposure to UV radiation minus the log of *E. coli* concentration after exposure to UV radiation, and the x-axis represents the UV dose applied to the microorganisms described in section 3.1.5.

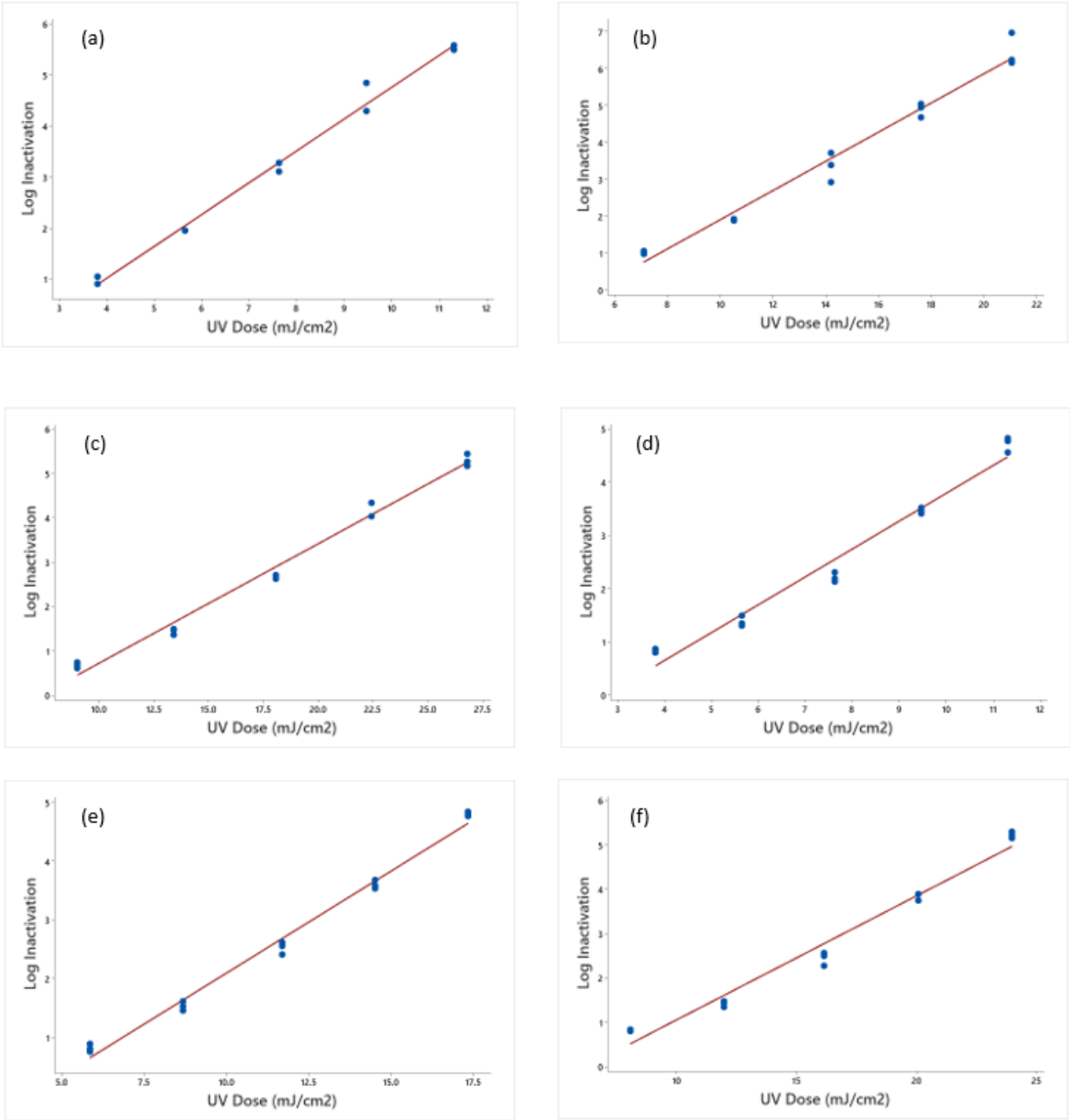

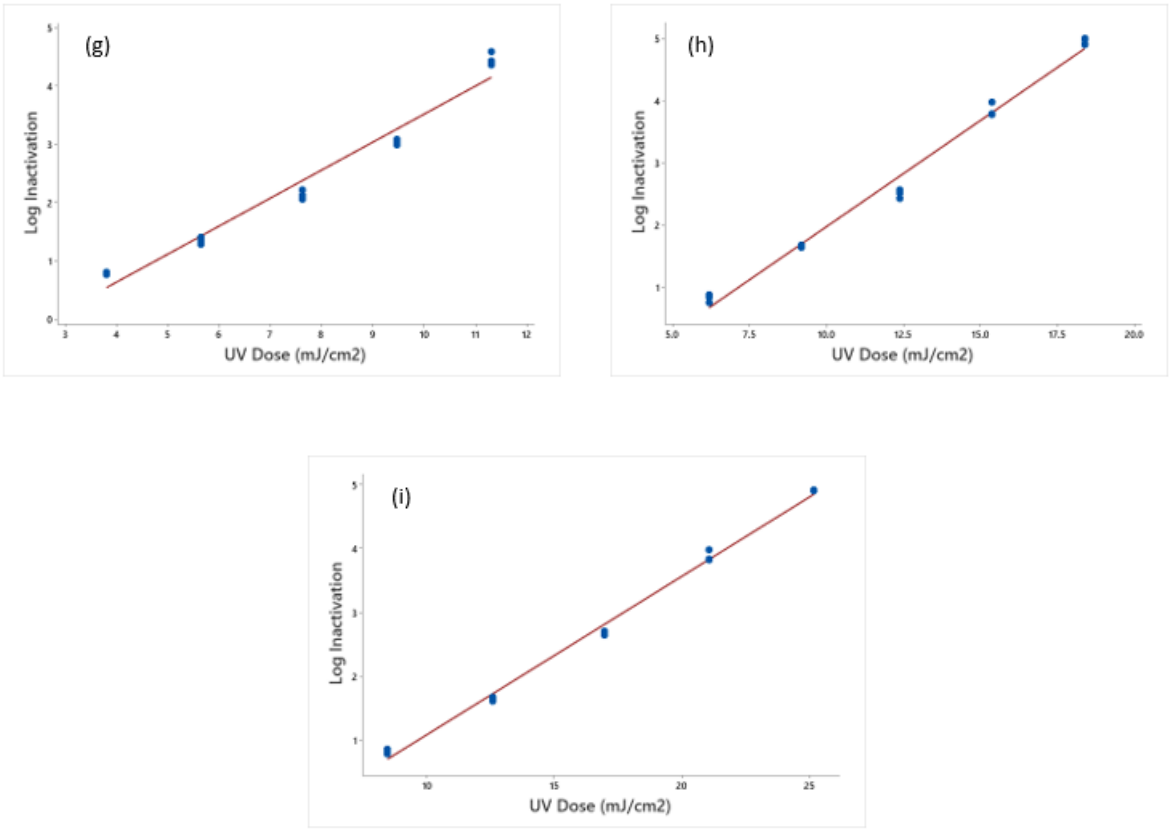

Figure 4.1: Dose-response curves of *E. Coli* without applying correction factors for 4 cm sample depth.

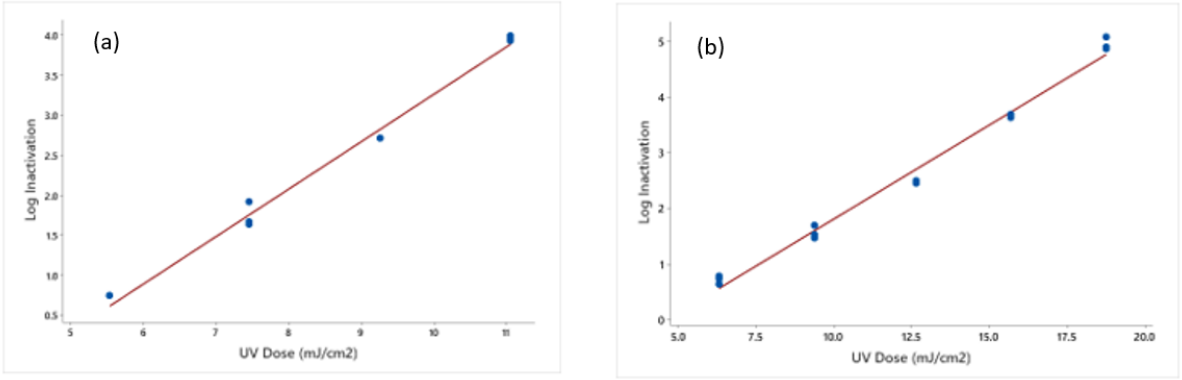

Figure 4.2: Dose-response curves of *E. Coli* without applying correction factors for 2.5 cm sample depth.

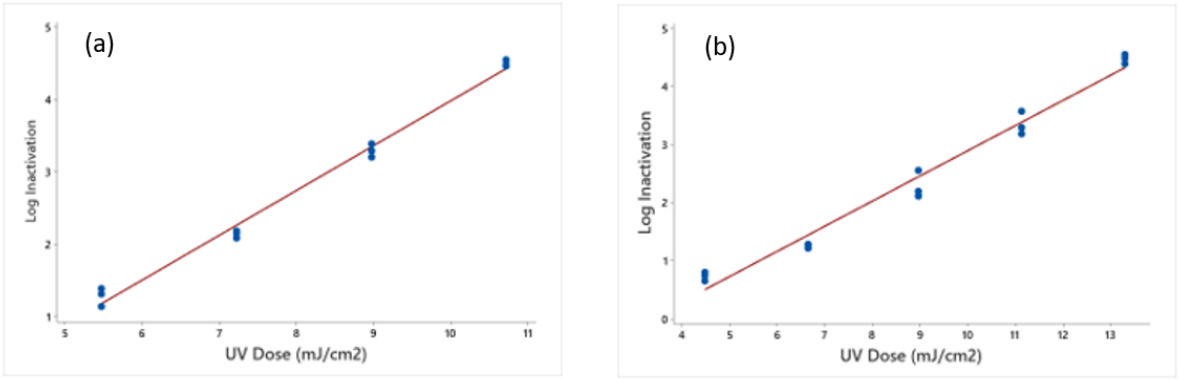

Figure 4.3: Dose-response curves of *E. Coli* without applying correction factors for 1 cm sample depth.

As expected, the higher the delivered dose, the higher the observed log inactivation. It can be seen from the graphs that there is a linear relation for each experiment between log inactivation and the applied UV dose, which was previously described by Chick and Watson (1908) in Equation 2.1. In addition, by comparing the graphs, it is evident that not only absorbance but also turbidity had a significant impact on UV disinfection performance which is consistent with the literature (Christensen and Linden, 2003; Liu and Zhang, 2006). More precisely, in Figure 4.1, for experiments with the presence of humic acid (b and c), a higher UV dose was required to achieve the same log inactivation compared to the first experiment when there was no humic acid and kaolinite. For example, to achieve 5-log inactivation in Figures 4.1.a and 4.1.b, UV doses of about 17 and 26 mJ/cm^2 were required, respectively, while to reach the same log inactivation for the first experiment, a UV dose of roughly 10 mJ/cm^2 was needed. In those samples with only kaolinite (d and g), the log inactivation slightly reduced compared to the first experiment, which can be attributed to the shielding effect of kaolinite particles for microorganisms that protect them from UV radiation. Also, in samples in which both humic acid and kaolinite were presented, it can be seen that the log inactivation of *E. coli* considerably decreased in all three different sample depths.

Moreover, from Figure 4.1.i, Figure 4.2.b, and Figure 4.3.b, it can be inferred that the depth of samples affected the dose-response curve. For example, in order to achieve a log reduction of 4 in all samples with a high concentration for humic acid and kaolinite, UV doses of approximately 22, 16.5, and 12.5 mJ/cm^2 were applied in sample depths of 4, 2.5, and 1 cm, respectively. Thus, UV disinfection was more efficient as the sample depth decreased.

In Table 4.2, the inactivation rate constants for each experiment obtained by LR analysis from the inactivation curves of experiments are presented. In Figure 4.4, the inactivation rate

constants for three sample depths were plotted against both turbidity and absorbance to indicate the combined effect of water quality parameters on UV inactivation.

Table 4.2: Inactivation rate constants k (cm^2/mJ) and R^2 (-) values obtained via LR analysis.

	Experiments	k (cm^2/mJ)	Intercept (-)	R^2	95% CI
4 cm sample depth	1	0.624	-1.480	0.990	(0.573, 0.674)
	2	0.396	-2.046	0.976	(0.359, 0.432)
	3	0.269	-1.974	0.986	(0.249, 0.288)
	4	0.524	-1.445	0.970	(0.469, 0.578)
	5	0.347	-1.383	0.990	(0.326, 0.369)
	6	0.279	-1.737	0.973	(0.251, 0.307)
	7	0.480	-1.290	0.966	(0.426, 0.534)
	8	0.342	-1.443	0.987	(0.318, 0.365)
	9	0.249	-1.408	0.995	(0.238, 0.259)
2.5 cm sample depth	1	0.592	-2.657	0.989	(0.542, 0.641)
	9	0.338	-1.568	0.9876	(0.315, 0.360)
1 cm sample depth	1	0.619	-2.213	0.991	(0.578, 0.660)
	9	0.434	-1.446	0.978	(0.394, 0.473)

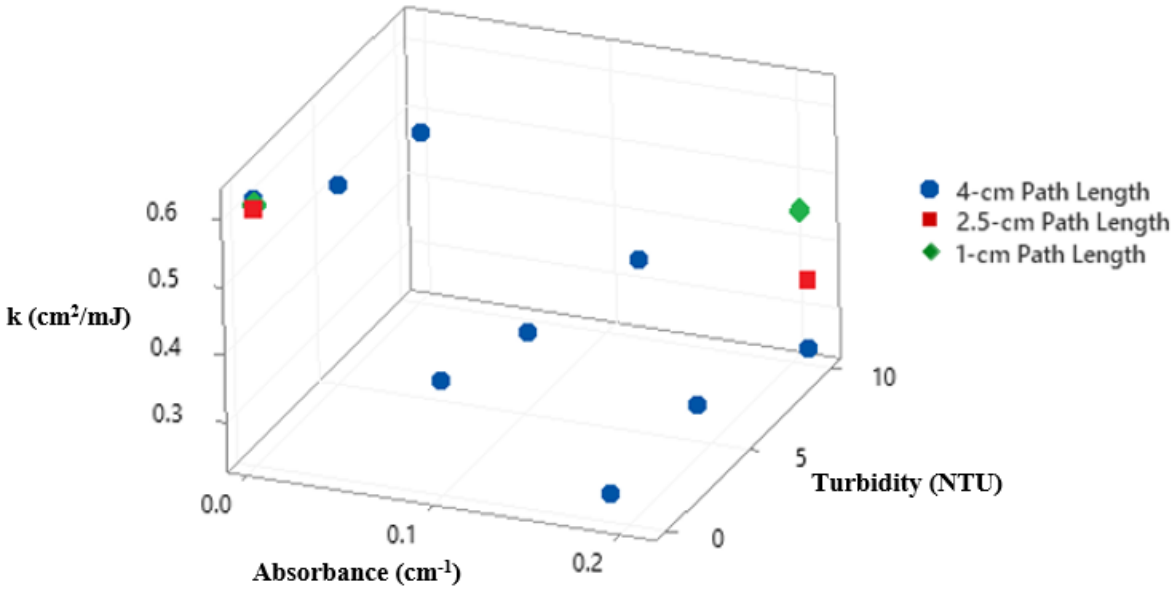

Figure 4.4: Inactivation rate constant plotted against turbidity and absorbance.

From Figure 4.4, it can be inferred that the inactivation rate constants decreased significantly from experiment #1 with only pure water matrix to experiment #9 with high concentrations of humic acid and kaolinite in all three sample depths. One of the reasons for this issue is the absorption of radiation by humic acid, leading to a reduction of radiation available for microorganism inactivation. For example, as the humic acid concentration increased from 0 mg/L in experiment #1 to 7 mg/L in experiment #3, the inactivation rate

constants dropped from 0.624 to 0.269 cm^2/mJ, respectively. The other reason is related to turbidity that affected UV disinfection by scattering UV light and protecting microorganisms from UV radiation. For instance, in experiment #1, the *E. coli* inactivation rate constant was 0.624 cm^2/mJ when turbidity was 0 NTU, while it reduced to 0.48 cm^2/mJ for turbidity of 10 NTU in experiment #7. Moreover, as discussed earlier, it can be seen that the inactivation rate constant of *E. coli* with the presence of high concentrations of humic acid and kaolinite was reduced from 0.434 to 0.249 cm^2/mJ as the sample depth increased from 1 to 4 cm. This could be attributed to the light that it could not travel completely through the entire depth when entered at the top of a deep volume.

In the next step, all the data obtained from UV inactivation experiments for the sample depth of 4 cm were analyzed to see the effect of turbidity, absorbance, and also their interactions. Generally, the interaction term indicates the effect of turbidity and absorbance on each other that as the light is scattered due to turbidity, it can affect to increase the amount of light to be absorbed. In this case, a complete GLM (GLM_1 – Equation 4.1) and a simplified GLM (GLM_2 – Equation 4.2) were obtained:

$$k = 0.000475\ T^2 + 3.23\ A^2 + 0.0703\ T \cdot A - 0.01799 \cdot T - 2.426 \cdot A + 0.6160 \qquad (4.1)$$

$$k = - 0.01341 \cdot T - 1.818\ A + 0.0761\ T \cdot A + 0.6021 \qquad (4.2)$$

Where k (cm^2/mJ) is the inactivation rate constant, T (NTU) is the measured turbidity level, and A (cm^{-1}) is the measured absorbance at wavelength 254 nm.

The statistical analysis resulted in a goodness-of-fit for both models in which the R-squared value for GLM_1 and GLM_2 were 98 % and 97%, respectively. Moreover, Table 4.3 and Table 4.4 summarized the analysis of variance for GLM_1 and GLM_2, respectively.

Table 4.3: Summarized analysis of variance for GLM_1.

Source	Contribution	P-Value
Turbidity	6.02%	0.079
Absorbance	86.89%	0.006
Turbidity*Turbidity	0.36%	0.506
Absorbance*Absorbance	2.00%	0.147
Turbidity*Absorbance	3.60%	0.053

Table 4.4: Summarized analysis of variance for GLM_2.

Source	Contribution	P-Value
Turbidity	6.02%	0.014
Absorbance	86.89%	0.000
Turbidity*Absorbance	4.27%	0.040

Since the p-value for absorbance is smaller than the set significance level (0.05), it is the only significant term of the model in the analysis of variance for GLM_1 which is not consistent with the previous studies; whereas the analysis of variance for GLM_2 determined that turbidity, absorbance, and also their interaction that caused to increase the inactivation rate constant, are significant since the p-values are less than the significance level and it can properly describe the inactivation rate constant.

Moreover, the adequacy of GLM_2 was evaluated through the analysis of residuals (Figure 4.5), which demonstrated that all assumptions at the base of the GLM analysis were met.

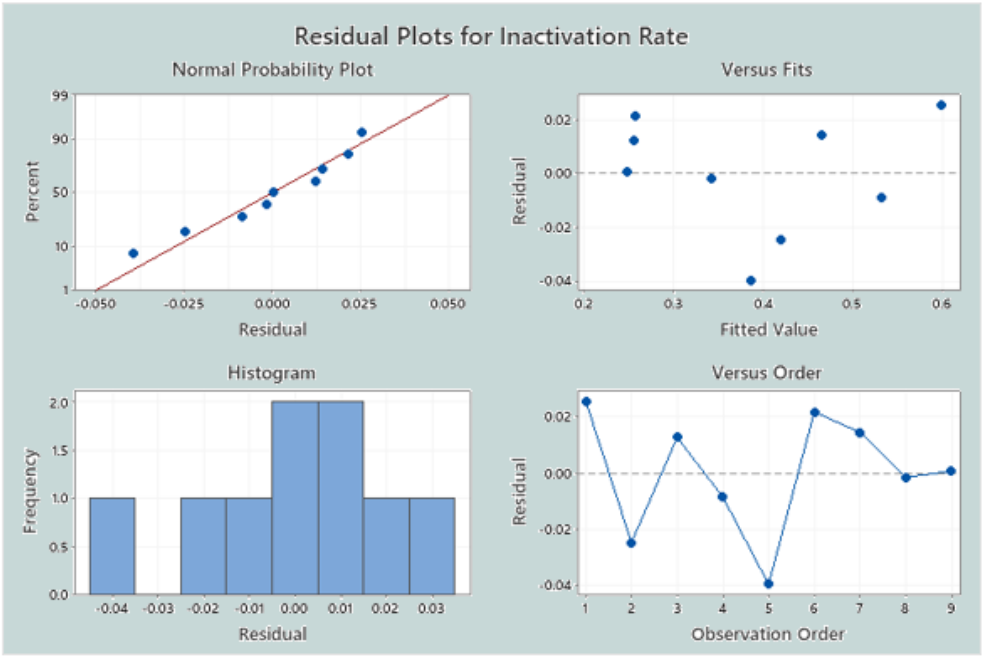

Figure 4.5: Results of the analysis of residuals conducted for the simplified GLM with Equation 4.2.

It can be seen from the normal probability plot that residuals are normally distributed because they follow a linear trend, while the histogram shows the skewness of data. The residual plot versus fits verifies the assumption that the residuals have constant variance and

the residual plot versus order plot verifies the assumption that the residuals are uncorrelated with each other.

From the statistical analysis, it can be concluded that the performance of UV disinfection is significantly influenced by absorbance, turbidity, and the interaction between them for the ranges considered in this work which is consistent with literature. For example, the results of Farrell et al. (2018) indicated that *E. coli* inactivation was significantly affected by absorbance with the presence of humic acid and Fe(III). Moreover, unlike MS2 coliphage that was not affected by turbidity (Batch et al., 2004), Liu and Zhang (2006) concluded that *E. coli* was influenced when turbidity was more than 4 NTU.

After investigating the effect of turbidity and absorbance by data analysis, in order to obtain the effective inactivation curve for *E. coli*, the corrected applied UV doses were calculated, considering all the correction factors described in section 3.1.6. The values of the corrected UV doses are reported in Tables 4.5 and 4.6. Also, Figure 4.6.a shows the inactivation curve for uncorrected UV dose. At the same time, Figure 4.6.b illustrates the dose-response curve with corrected applied UV doses obtained by LR analysis for the sample depth of 4 cm.

Table 4.5: Average log inactivations (-) achieved with corrected applied UV doses (mJ/cm^2) for all nine experimental conditions for 4 cm sample depth.

4 cm Sample Depth					
UV Dose (mJ/cm^2)	**EX1**	**UV Dose (mJ/cm^2)**	**EX2**	**UV Dose (mJ/cm^2)**	**EX3**
3.1	0.98	3.8	1.03	3.50	0.68
4.6	1.95	5.65	1.91	5.20	1.44
6.2	3.20	7.61	3.35	7	2.66
7.7	4.57	9.50	4.90	8.70	4.23
9.2	5.53	11.30	6.47	10.40	5.29
UV Dose (mJ/cm^2)	**EX4**	**UV Dose (mJ/cm^2)**	**EX5**	**UV Dose (mJ/cm^2)**	**EX6**
3.1	0.83	3.1	0.81	3.1	0.84
4.6	1.38	4.6	1.53	4.6	1.42
6.2	2.21	6.2	2.53	6.2	2.45
7.7	3.47	7.7	3.60	7.7	3.79
9.2	4.72	9.2	4.80	9.2	5.22
UV Dose (mJ/cm^2)	**EX7**	**UV Dose (mJ/cm^2)**	**EX8**	**UV Dose (mJ/cm^2)**	**EX9**
3.1	0.78	3.1	0.83	3.1	0.82
4.6	1.34	4.6	1.66	4.6	1.64
6.2	2.13	6.2	2.51	6.2	2.67
7.7	3.03	7.7	3.85	7.7	3.88
9.2	4.45	9.2	4.96	9.2	4.91

Table 4.6: Average log inactivations (-) achieved with corrected applied UV doses (mJ/cm^2) for experimental conditions for 2.5 cm and 1 cm sample depth.

2.5 cm Sample Depth			
UV Dose (mJ/cm^2)	**EX1**	**UV Dose (mJ/cm^2)**	**EX9**
3.1	-	3.1	0.72
4.6	0.75	4.6	1.57
6.2	1.74	6.2	2.47
7.7	2.72	7.7	3.66
9.2	3.97	9.2	4.95
1 cm Sample Depth			
UV Dose (mJ/cm^2)	**EX1**	**UV Dose (mJ/cm^2)**	**EX9**
3.1	-	3.1	0.73
4.6	1.28	4.6	1.25
6.2	2.14	6.2	2.28
7.7	3.30	7.7	3.35
9.2	4.50	9.2	4.48

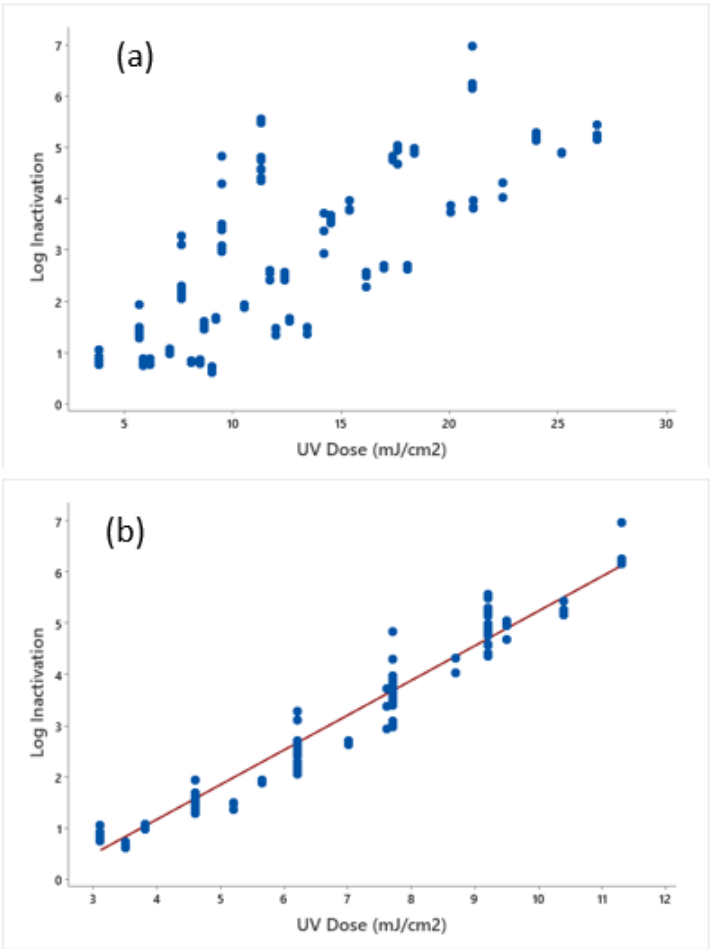

Figure 4.6: Log inactivation plotted (a) against uncorrected applied UV dose (b) corrected applied UV dose.

From the first graph, it can be inferred the importance of correction factors in obtaining a linear dose-response curve, and it is evident that without considering any correction factors, three linear trends are observed. The second graph indicates that the correction factors proposed by Bolton and Linden (2003) were able to correct the applied UV doses, obtaining a linear distribution of the data. In this case, the relation between log inactivation and UV dose is defined by Equation 4.3.

$$\text{Log Inactivation} = 0.6785 \cdot \text{UV Dose} - 1.5407 \qquad (4.3)$$

In addition, the residual plots for log inactivation of these data are shown in Figure 4.7. From the normal probability plot, it can be seen that some data do not follow the linear regression curve, which could be attributed to the scattering effect related to the kaolinite particles.

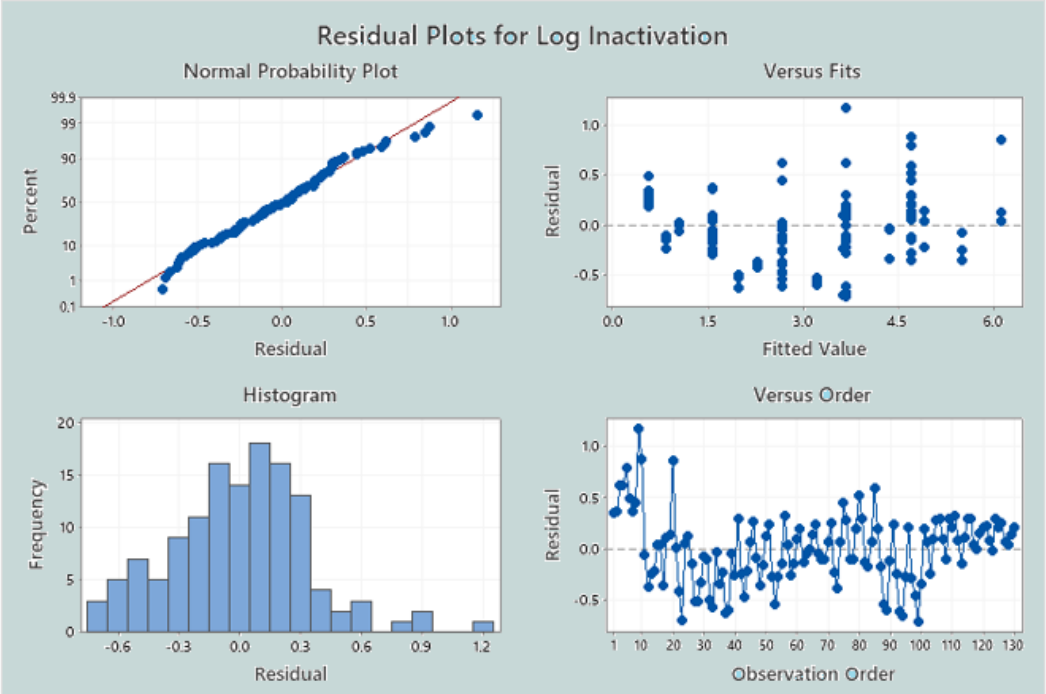

Figure 4.7: Analysis of residuals for the LR model defining the inactivation curve.

In general, the inactivation curve defined with Equation 4.3 was consistent with the inactivation curves determined by Sommer et al. (2000) and Oguma et al. (2002). However, it is noticeable that the obtained inactivation rate constant in this study is slightly greater than the ones reported in literature (Table 4.7). This could be due to the type of *E. coli* used in those research works, which was different compared to the one employed in this work.

Table 4.7: *E. coli* inactivation rate constants, with R^2 values, for the LR obtained from experimental data in this study and for the inactivation curves determined by studies present in literature.

Data Source		UV Dose Range (mJ/cm^2)	Inactivation Rate (cm^2/mJ)	R^2 (%)
Inactivation Experiments		3.1 - 11.30	0.678	95
Literature	Sommer et al. (2000)	1 - 7	0.642	85
	Oguma et al. (2002)	1.5 - 9	0.539	64

Based on the hypothesis that bacterial inactivation is related to the applied UV dose, a comparison between the corrected applied UV doses and GLM obtained from data analysis (Equation 4.2) was carried out. Firstly, by having the turbidity and absorbance values defined in the experimental design, the inactivation rate constants were estimated based on the GLM (Equation 4.2). Then, in order to obtain the relative values, the ratio between obtained inactivation rate constant in each experiment and experiment #1 was determined. Similarly, the relative UV doses were calculated. In Table 4.8, the relative UV doses and relative inactivation rate constants are presented. As the relative inactivation rate constants are estimated using the raw data without applying any correction factor, the relative UV doses can be compared to them to assess whether the correction factor can accurately estimate the effective UV doses.

Table 4.8: Comparison between the relative UV doses obtained from experiments and relative inactivation rate constants obtained from GLM.

	Experiment	Relative UV Dose Obtained from Experiments	Relative k Obtained from GLM	Δ_{EXP-k}
4 cm Sample Depth	1	1	1	0
	2	0.66	0.70	-0.04
	3	0.48	0.43	0.05
	4	1	0.89	0.11
	5	0.65	0.65	0
	6	0.47	0.43	0.04
	7	1	0.78	0.22
	8	0.62	0.57	0.05
	9	0.45	0.41	0.04
2.5 cm Sample Depth	1	1	-	-
	9	0.59	-	-
1 cm Sample Depth	1	0.098	-	-
	9	0.096	-	-

It can be inferred that the correction factors proposed by Bolton and Linden (2003) adequately work for samples with different absorbance ranges. However, they are not sufficient to correct the applied UV doses when there is a turbid but poorly absorbing sample. It was

expected that relative values for UV doses and inactivation rate constants estimated by GLM were approximately the same for all conditions. While as the turbidity increased from 0 in experiment #1 (without any kaolinite and humic acid) to 10 NTU in experiment #7 (with only kaolinite), the differences considerably increased. This result indicates that another correction factor is required to estimate the delivered UV dose to microorganisms precisely.

4.2 UV Disinfection Modeling

4.2.1 Collimated Beam Apparatus Modeling

CB apparatus was modeled considering radiative transfer behavior to determine the average germicidal UV dose throughout the sample and compare it with the one calculated according to correction factors proposed by Bolton and Linden (2003). Both hexahedral and tetrahedral meshes of roughly 1 million with a good quality determining accurate solutions were generated for the domain (Figure 4.8). The convergence criterion for residual values in the CFD simulations was set to 10^{-8}.

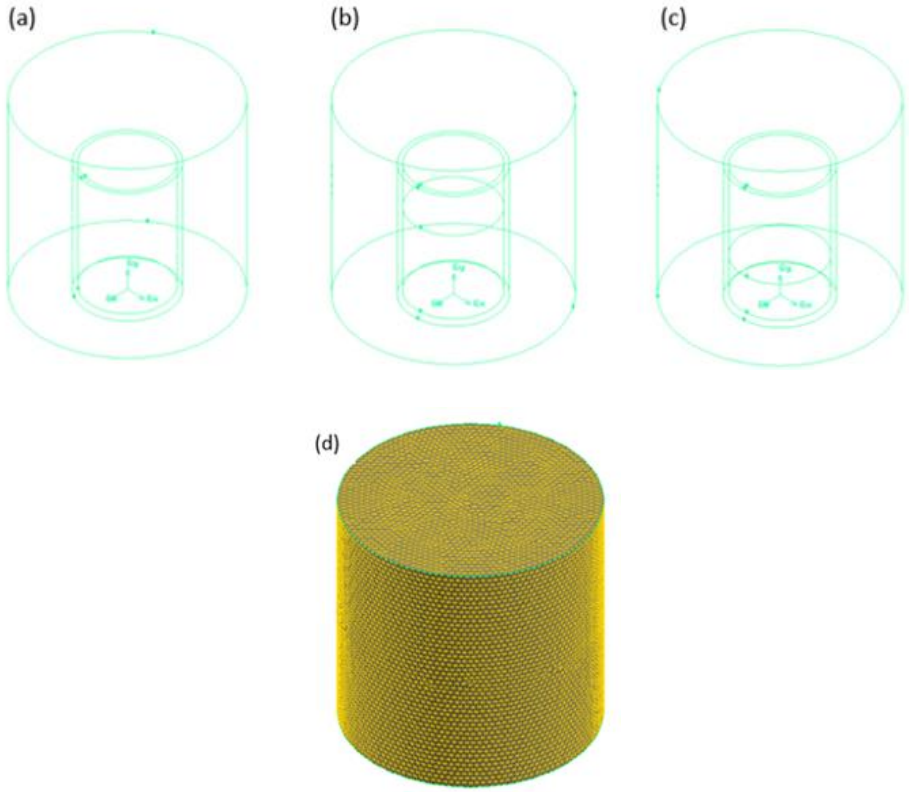

Figure 4.8: Geometric model of the CB apparatus for (a) 4 cm sample depth, (b) 2.5 cm sample depth, (c) 1 cm sample depth, and (d) the generated volume mesh.

Figure 4.9 shows that intensity across the sample surface was compatible with the results obtained by experiments using the radiometer for calculating the Petri factor. This ensured an overall consistency of the results from the calibrated radiation model with the experimental data.

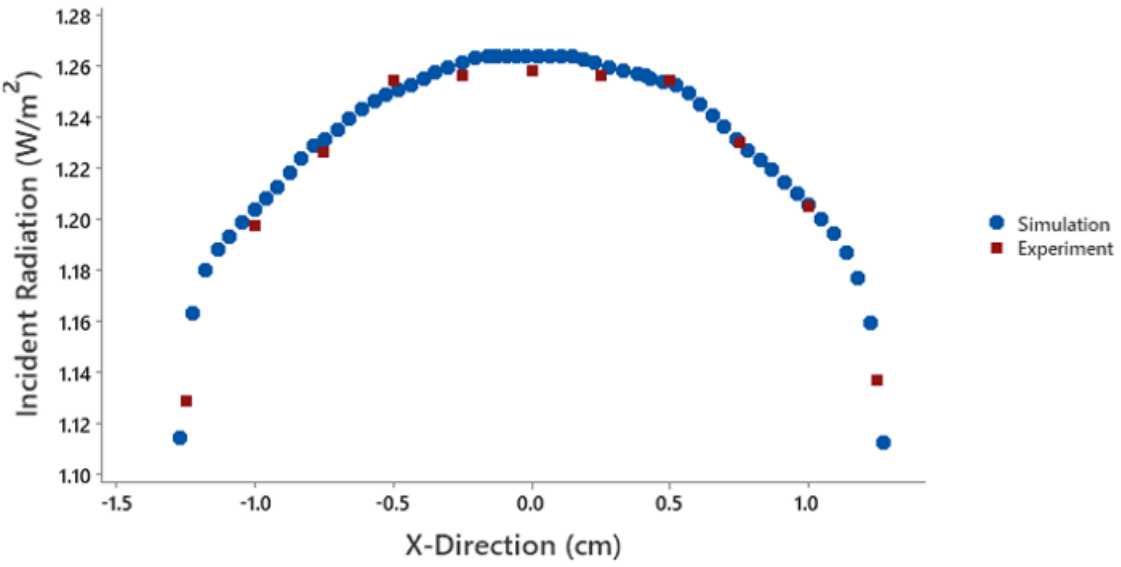

Figure 4.9: Intensity distribution across the sample surface in X-direction.

The UV fluence distribution modeling inside the sample was carried out for all experiments defined in the experimental design (Table 3.1). After defining the materials and assigning them to the model, the results indicated that as the UV radiation passed throughout the sample from the sample surface to the bottom, a fluctuation was observed, which was not as expected according to the Beer-Lambert equation. It is evident from Figure 4.10 that as UV radiation applied to the sample, its intensity decreased, and all of a sudden, by passing through the depth, it increased and then declined. This could be attributed to overestimating some reflection phenomena by software because of difficulty in simulating the radiation beam.

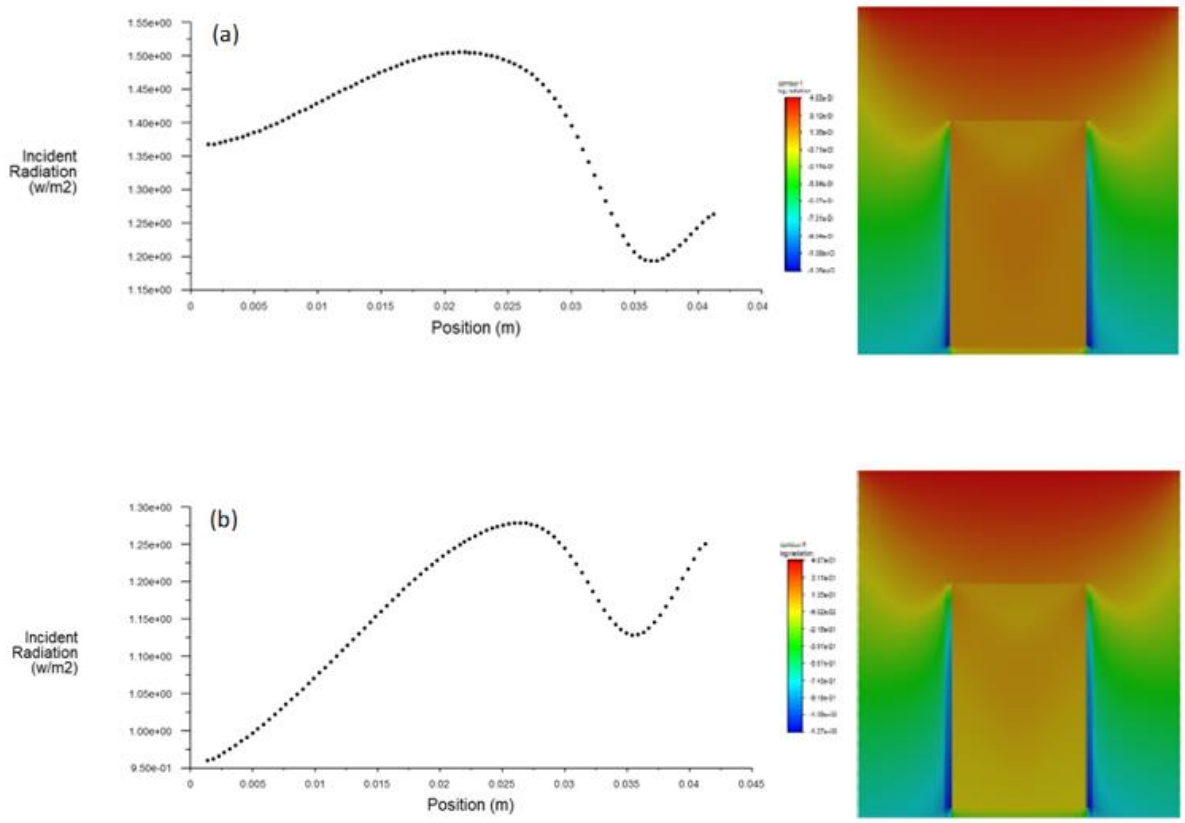

Figure 4.10: vertical radiation intensity and UV fluence distribution in the samples for (a) experiment #1 and (b) experiment #9.

Then, by improving the model and considering the thickness of glassware used in the inactivation experiments as an opaque radiation boundary condition, the simulations were performed for all experimental conditions defined in the experimental design. Figures 4.11 and 4.12 illustrate the vertical radiation intensity and UV radiation distribution throughout the sample for experiment #9, respectively. The other simulated experiments had the same trend as the ones shown in Figures 4.11 and 4.12.

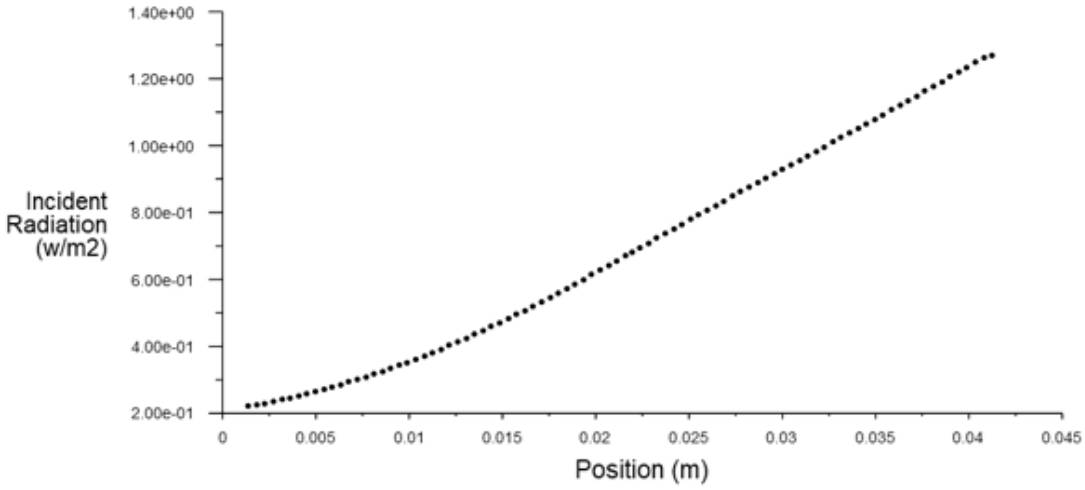

Figure 4.11: Vertical radiation intensity for experiment #9 defined in the DoE.

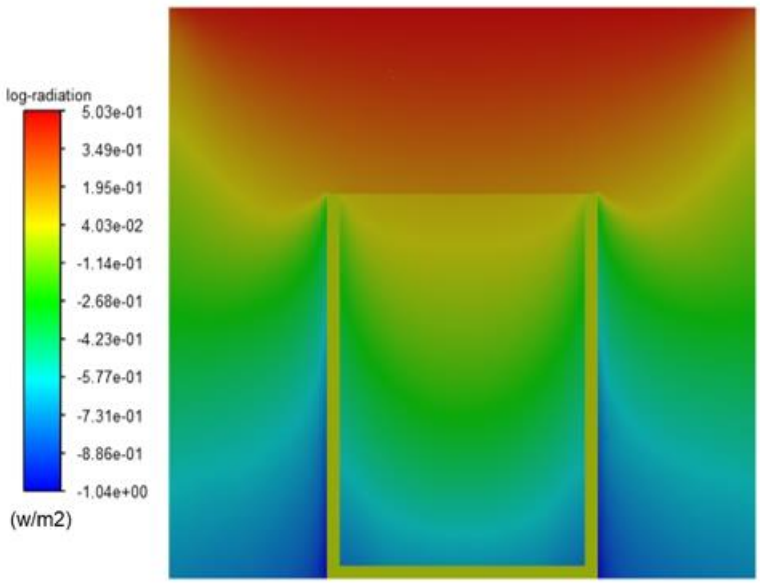

Figure 4.12: UV fluence distribution in sample for experiment #9 defined in the DoE.

As it was expected, the UV radiation intensity decreased by passing from the sample surface to the bottom, which shows that the pathogens in the deeper part of the sample can be exposed to less intensity. Finally, by multiplying the average radiations obtained from CFD simulations in the sample volumes by the exposure times calculated from Equation 3.5, the applied UV doses were estimated and the UV dose-response curve for sample depth of 4 cm was determined as illustrated in Figure 4.13.

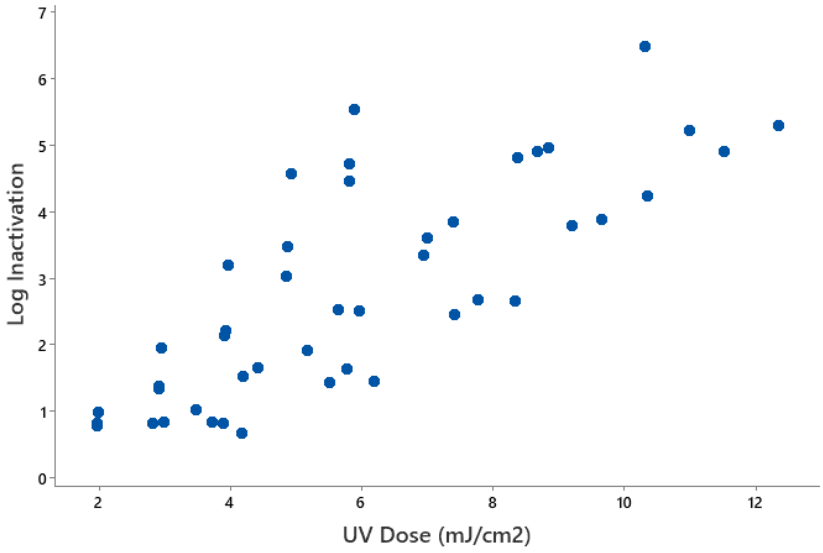

Figure 4.13: UV dose-response curve obtained from CFD simulations.

As it is evident from the graph, all the obtained outcomes did not follow one linear trend, unlike what was observed for experiments considering correction factors proposed by Bolton and Linden (2003). This is due to the lower average radiation estimated by the CFD simulations for pure water matrix and samples containing only kaolinite. Thus, it can be inferred that CFD software was not able to simulate the CB apparatus properly. It was expected that the DO model was able to provide an accurate prediction of applied radiation intensity and UV dose with respect to the Beer-Lambert simplified model. However, this was not the case, even though the simulations were performed appropriately. This could be attributed that the DO model is not able to model radiative transfer for collimated radiation accurately. In this regard, further studies would be necessary to investigate more in-depth the CB apparatus modeling, for example, by performing the simulations with a smaller setup, improving the description of the glass, and considering different values for angular discretization in the radiation model.

4.2.2 UV Disinfection Reactor Modeling

The UV disinfection reactor was modeled by coupling fluid dynamic and UV fluence rate results over a domain of discrete solid angels to determine the UV dose distribution in the reactor as a result of optical properties (turbidity and absorbance). It should be mentioned that the reactor fluid dynamic was thoroughly validated with a tracer test by Baldasso (2020).

In Figures 4.14.a and 4.14.b, the geometric model of the UV disinfection reactor and the generated volume mesh are illustrated, respectively.

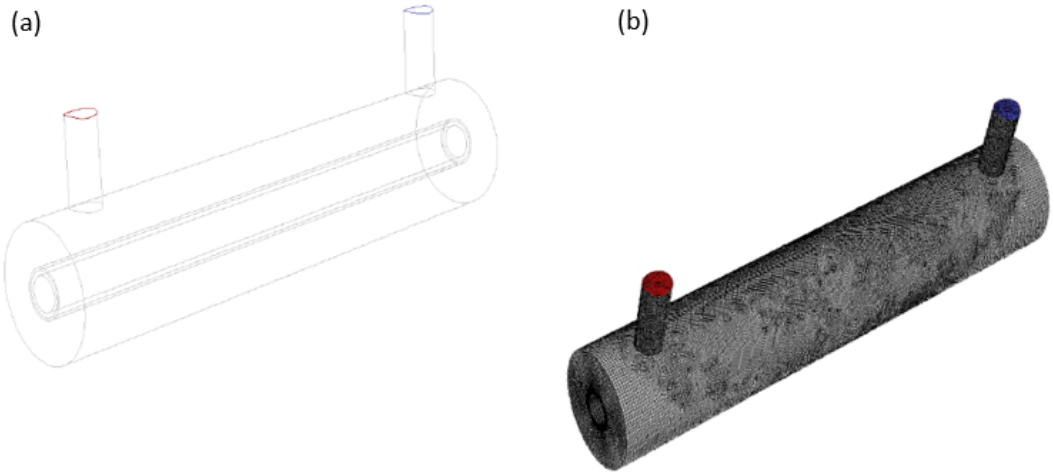

Figure 4.14: (a) Geometric model and (b) generated volume mesh for the UV disinfection reactor.

Figure 4.15 shows the simulated UV fluence rate distribution from the outer surface of the quartz sleeve to the one side of the reactor wall. It can be seen from Figure 4.15.a that the distribution curves are approximately the same while the turbidity changed in the water matrices from 0 NTU in experiment #1 to 5 NTU in experiment #4, only with slight differences, which is basically due to the scattering effect of particles. More precisely, as the UV radiations reach the particles, the light is scattered in every direction according to the Henyey-Greenstein scattering phase function, leading to an increase in the pathway of UV light in the reactor chamber before reaching the walls and being absorbed, which increases the UV fluence rate in experiment #4. Similarly, this effect can be seen by comparing experiments #2 and #5 with the same absorbance and different turbidity levels, leading to an increase in UV fluence rate. Moreover, it is evident that, due to higher absorbance in experiments #2 and #5 compared to experiments #1 and #4, a lower UV fluence rate was observed, which is expected to inactivate microorganisms with less efficiency. The same trend for two different water matrices used in the installed prototypes in Mexico with different optical properties is shown in Figure 4.15.b. In addition, these results are shown in Figure 4.16 by UV fluence rate contour plots along the longitudinal plane of the reactor.

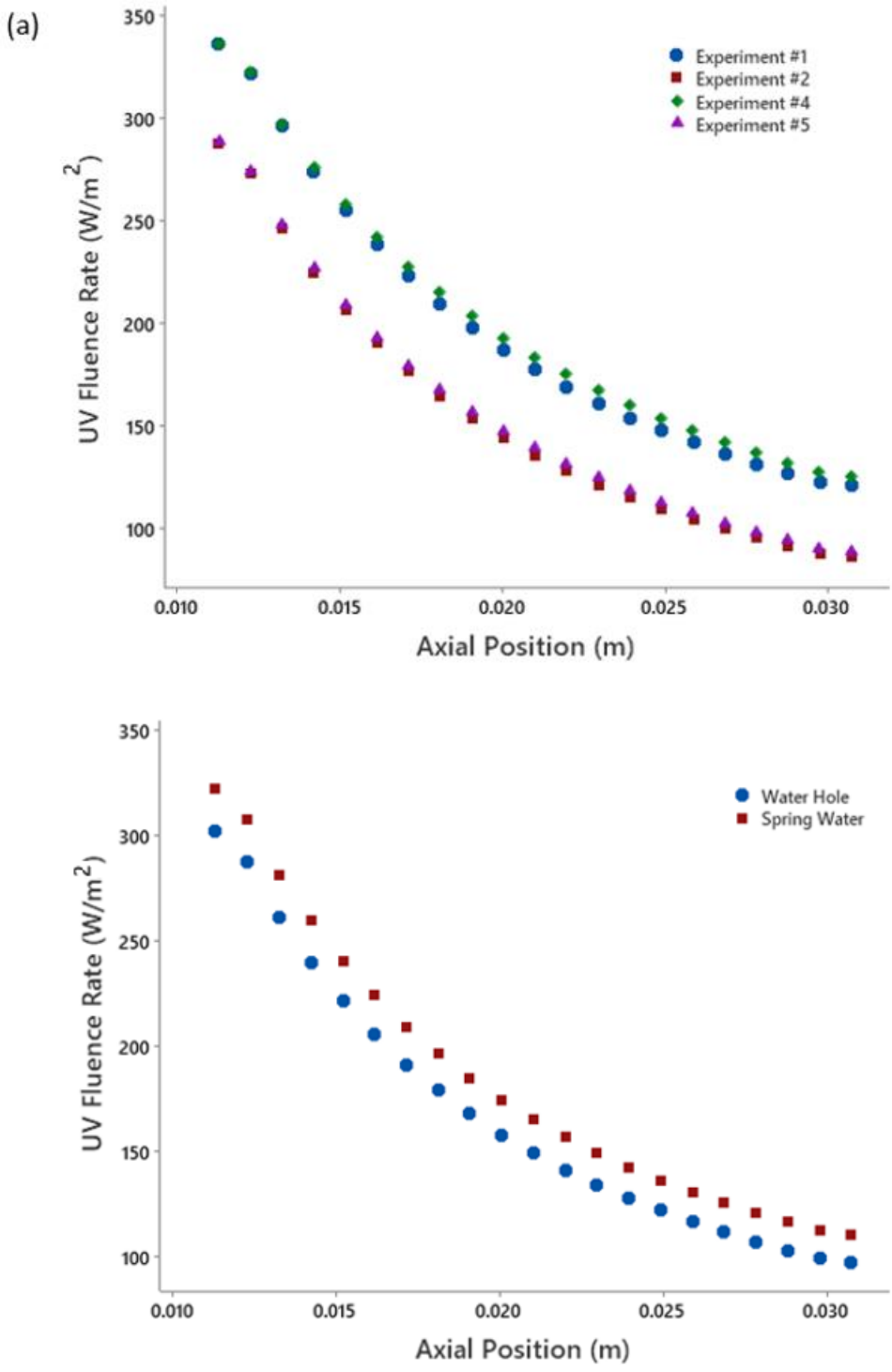

Figure 4.15: Simulated UV fluence rate distribution from the outer surface of quartz sleeve to the one side of the reactor wall (a) for experiments #1, #2, #4, and #5 (b) for water hole and spring water sources.

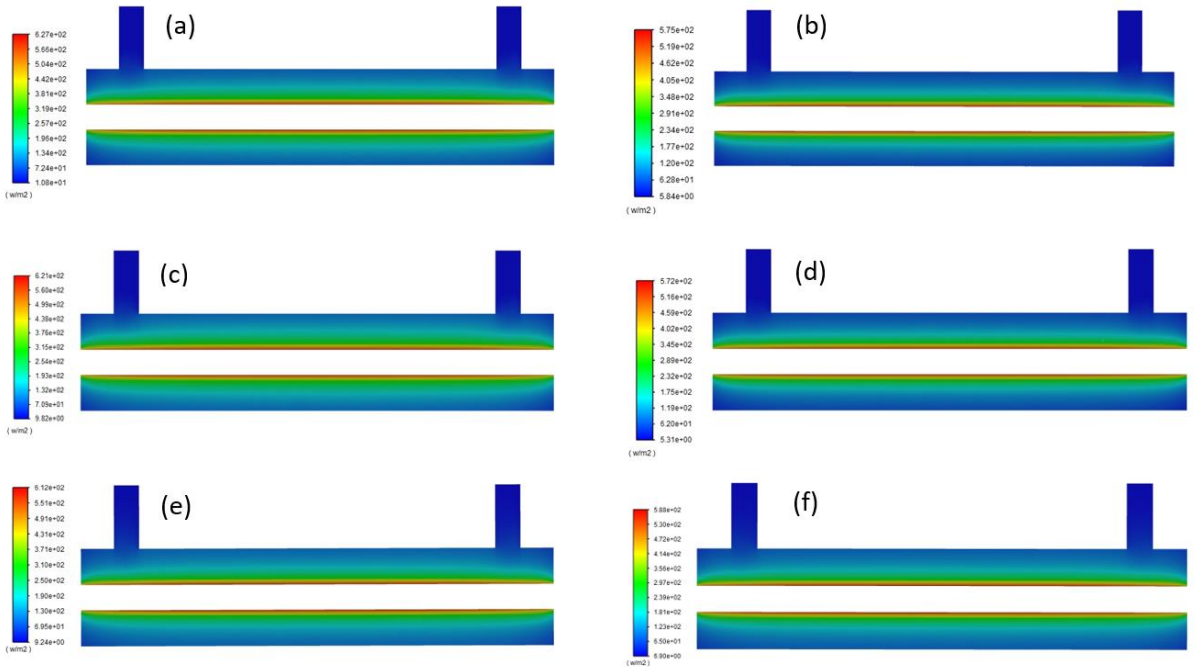

Figure 4.16: Simulated UV fluence rate distribution from UV lamp surface to the reactor walls for (a) experiment #1, (b) experiment #2, (c) experiment #4, (d) experiment #5, (e) spring water, and (f) hole water source.

In Figure 4.17, particle trajectories for experiments computed with the Lagrangian particle tracking method based on the absorbed UV fluence are shown. It can be seen that higher UV doses are observed for particles moving in the proximity of the lamp surface.

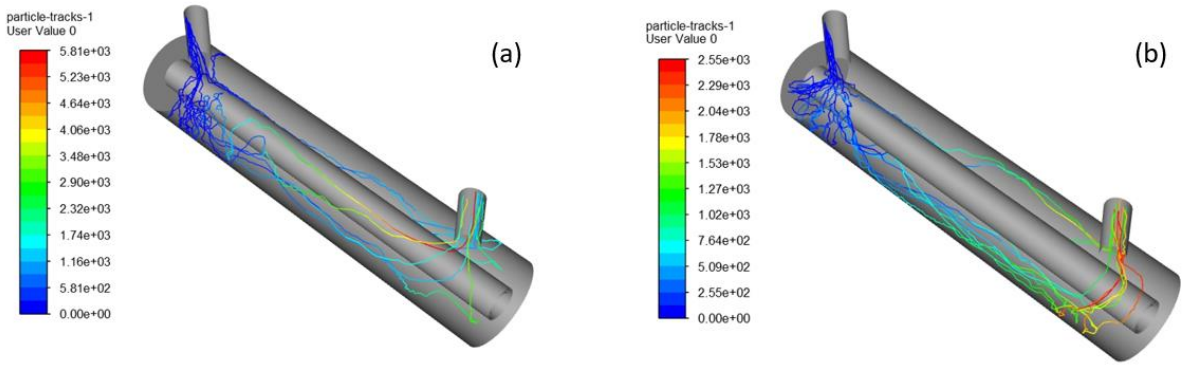

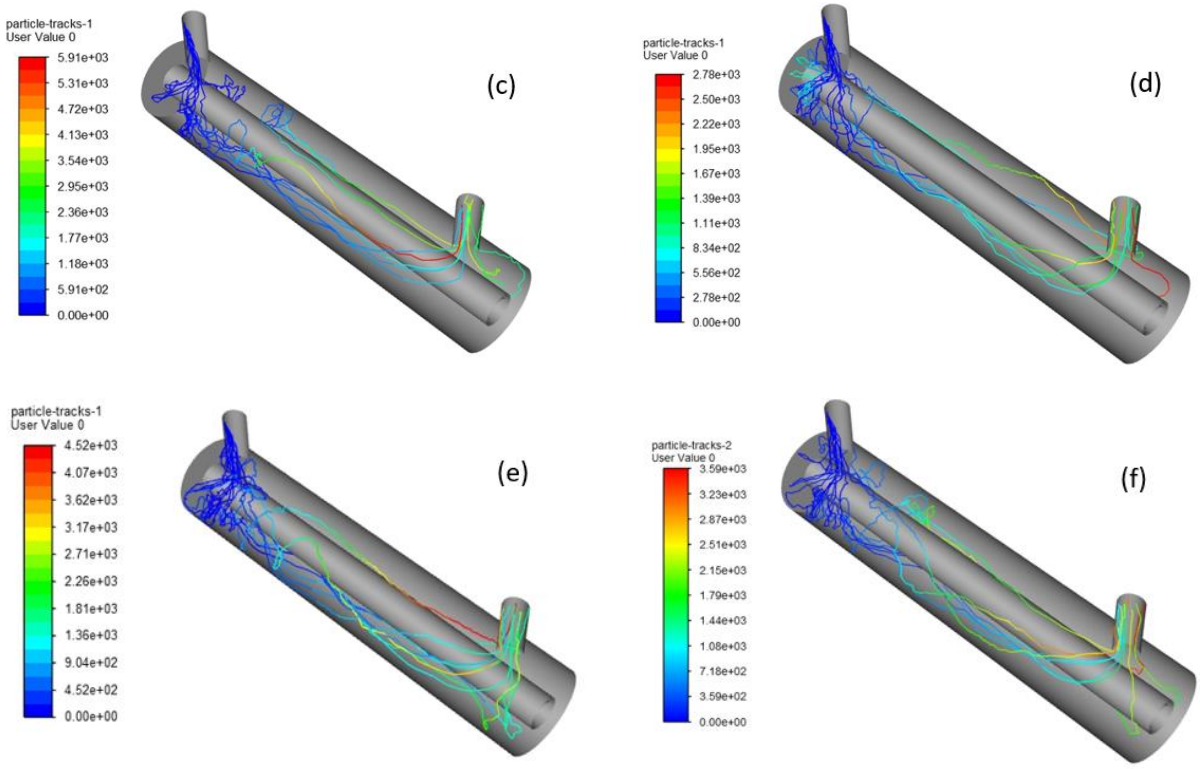

Figure 4.17: Particle trajectories for (a) experiment #1, (b) experiment #2, (c) experiment #4, (d) experiment #5, (e) water spring, and (f) water hole source computed with the Lagrangian particle tracking method based on the absorbed UV fluence.

In Figure 4.18, the simulated UV dose distributions for each experiment with different flowrates are shown. As it can be seen, more UV dose distribution curves of the simulated experiments are positioned to the left, which determine a smaller UV dose is absorbed by the particles. It is evident that as the flowrate increased, a lower UV dose was delivered to the particles. This could be due to the decrease of residence time in the reactor chamber for high flowrates. Also, it can be inferred that as the optical properties of water matrices (turbidity and absorbance) increased, the UV dose distribution curves shifted towards the lower UV dose values. By comparing the statistical parameters of the simulated UV dose distributions for the experiments, the differences can be observed. In Table 4.9, these statistical parameters (weighted mean, median, and mode) are presented.

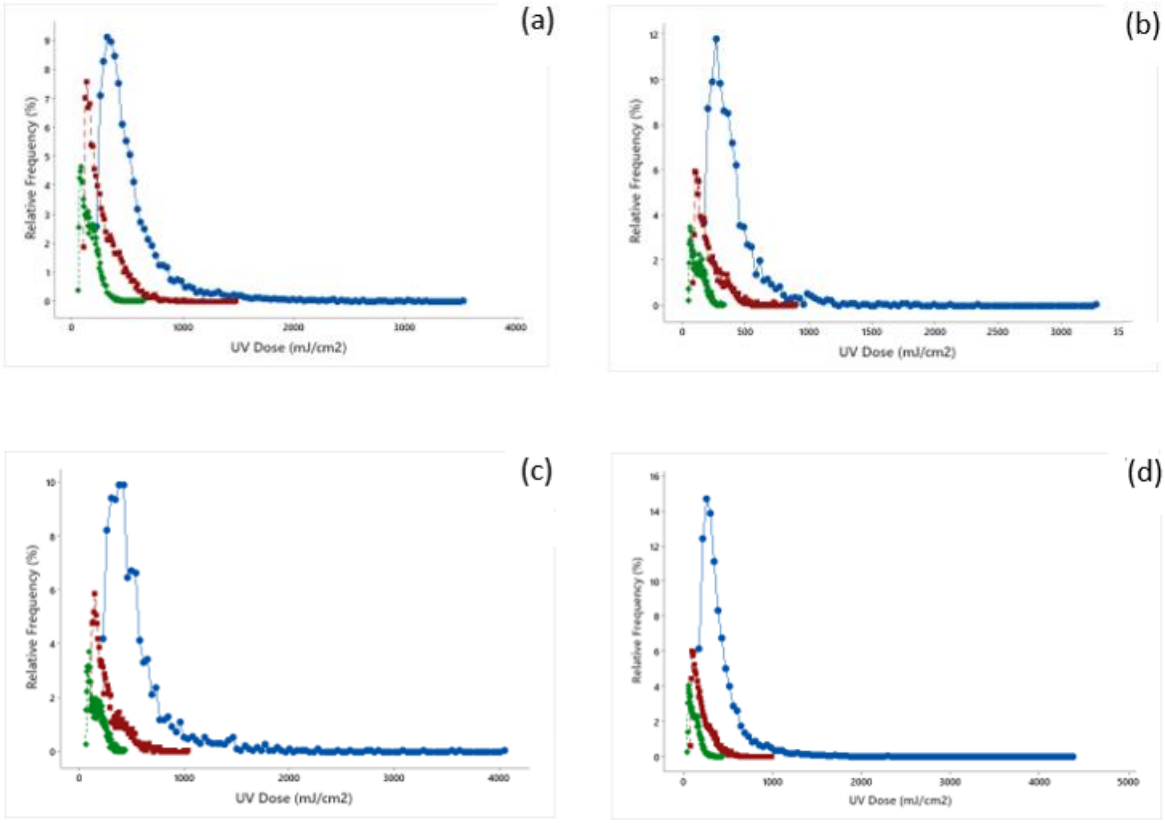

Figure 4.18: UV dose distribution curves for (a) experiment #1, (b) experiment #2, and (c) experiment #4, and (d) experiment #5 for flowrates of 1.5 L/min (blue), 3 L/min (red), and 5.2 L/min (green).

Table 4.9: Statistical parameters (mJ/cm^2) of simulated UV dose distributions for the three tested flowrates for experiments #1, #2, #4, and #5.

Experiment #	Statistical Parameters	Flowrates (L/min)		
		1.5	3	5.2
1	Weighted Mean	520	270	156
	Median	419	231	146
	Mode	319	134	81
2	Weighted Mean	394	206	119
	Median	327	169	113
	Mode	265	95	53
4	Weighted Mean	533	263	155
	Median	458	222	145
	Mode	419	147	93
5	Weighted Mean	416	212	123
	Median	350	183	113
	Mode	265	100	61

As it can be seen, the statistical parameters for experiments #1 (pure water with no turbidity and absorbance) and #4 (with the only turbidity of 5 NTU) are approximately the

same, with only a slightly greater weighted mean value for experiment #4 related to flowrates of 1.5 L/min, which is due to the scattering effect of particles and led to an increase in weighted mean value which was described entirely earlier. Similarly, this effect can be seen by comparing experiments #2 and #5 with the same absorbance and different turbidity levels that led to an increase of weighted mean of UV does in experiment #5. Moreover, a comparison between statistical parameters of experiments #1 and #4 indicates that the impact of turbidity was insignificant, expecting to have roughly the same log inactivation for these two experiments. While as absorbance increased in experiments #4 and #5, according to the statistical parameters, it can be inferred that absorbance significantly affected the UV disinfection performance, which can probably result in delivering less UV dose to pathogens.

Similarly, the simulated UV dose distribution curves for household treatment system prototypes installed in Mexico with two different water sources shift to the left (Figure 4.19), determining that particles absorbed on average a smaller UV dose. As it is shown in Table 4.10, the statistical parameters of the spring water source are greater than those of the water hole source, which was due to the lower optical properties of the water matrix in the spring water source, led to deliver a greater UV dose to the particles in the spring water source. As a result, it is expected to have more efficient UV disinfection than the water hole source.

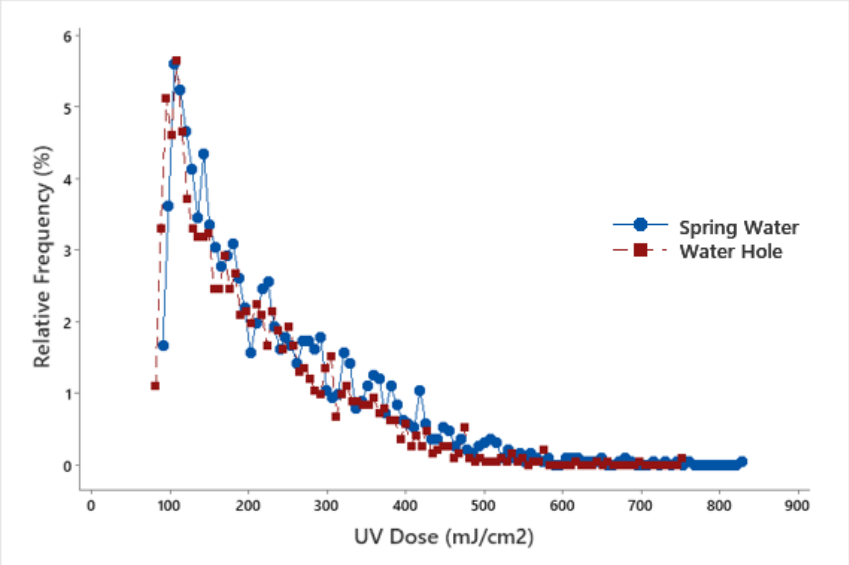

Figure 4.19: UV dose distribution curves for two different water sources with the flowrate of 3.3 L/min.

Table 4.10: Statistical parameters (mJ/cm^2) of simulated UV dose distributions for two different water sources with the flowrate of 3.3 L/min

Water Sources	Statistical Parameters	
Spring Water	Weighted Mean	224
	Median	187
	Mode	105
Water Hole	Weighted Mean	203
	Median	176
	Mode	108

Finally, by using the simulated UV dose distribution and *E. coli* inactivation curve obtained through the inactivation experiments using the bench-scale CB apparatus, the predicted log inactivation was calculated. As the applied UV doses in the simulated UV disinfection reactor were extremely high, it resulted in inactivating all microorganisms. To this end, the predicted log inactivation values of a more resistant pathogen to UV radiation, MS2 coliphage, are provided in Table 4.11 for experiments #1, #2, #4, and #5 with different flowrates. The MS2 log inactivation kinetic model used for predicting the log inactivation values in this study was obtained from the research done by Baldasso (2020).

Table 4.11: Predicted MS2 log inactivation values for each flowrate tested for experiments #1, #2, #4, and #5.

Experiment #	Flowrate (L/min)	Log Inactivation
1	1.5	6.51
	3	3.27
	5.2	2.70
2	1.5	5.10
	3	2.70
	5.2	2.63
4	1.5	6.56
	3	3.34
	5.5	2.71
5	1.5	5.21
	3	2.64
	5.2	2.65

As it can be seen, the log inactivation values for all experiments reduced as the flowrates increased from 1.5 to 5.2 L/min. Moreover, as expected, experiments #1 and #4 had higher log inactivation values than other experiments. The log inactivation values for three flowrates in

experiment #4, which contains only kaolinite particles with the turbidity of 5 NTU were comparable to experiment #1, indicating that the effect of turbidity was insignificant on UV disinfection performance. While the results for experiments #2 and #5 with higher absorbance values led to less efficient disinfection by UV radiation compared to experiments #1 and #4, which shows the significant impact of absorbance on UV inactivation. Moreover, as the scattering effect in water matrices with different optical properties was described by comparing the statistical parameters, the log inactivation results for those experiments with turbidity were slightly higher than those without scattering. It should be noted that the simulated results confirmed the findings of Baldasso (2020) and Batch et al. (2004) through the MS2 inactivation experiments by CB apparatus that the only significant parameter was absorbance.

In Table 4.12, both field results and predicted results of log inactivation of MS2 coliphage for household water treatment system prototypes installed in Mexico are illustrated.

Table 4.12: Predicted and field results of MS2 log inactivation values for prototypes installed in Mexico.

Water Source	Flowrate (L/min)	Predicted Log Inactivation	Field Results of Log Inactivation	$\Delta_{SIM-EXP}$
Spring Water	3.3	3.38	4.13	- 0.75
Water Hole	3.3	3.14	3.66	- 0.52

The results show that the log inactivation of the spring water source was greater than the one for the water hole source due to the lower optical properties (turbidity and absorbance), which is consistent with the obtained experimental results. The comparison between simulations and field results indicated that the predicted log inactivation values of the spring water and the water hole sources were slightly lower than the field experiments. These minor differences can be attributed to specific measuring errors occurring during the experiments, the accuracy of CFD software to model the UV dose distribution inside the reactor, particle characteristics, or even the MS2 inactivation kinetic model. However, the modeling results of the UV disinfection reactor determined that CFD simulations could effectively predict inactivation results for MS2 obtained during field experiments on two different real water matrices.

CHAPTER 5. CONCLUSIONS AND FUTURE DEVELOPMENTS

This study aimed at (i) investigating the turbidity and absorbance effect on LP UV inactivation of spiked E. *coli* in three different sample depth conditions (1, 2.5, and 4 cm) using a standard bench-scale CB apparatus, (ii) modeling the effect of turbidity and absorbance on UV radiation in CB apparatus, and (iii) modeling the effect of turbidity and absorbance on *E. coli* and MS2 inactivation in a small-scale UV disinfection reactor for the decentralized household treatment of drinking. The conclusions obtained from this study and future research recommendations to further assess the applicability of UV disinfection for water and wastewater treatment are addressed in this chapter which are as follows:

- In all experiments conducted by CB apparatus for three different sample depths, the spiked laboratory-grown *E. coli* with the initial concentration of 10^6-10^7 CFU/ml was effectively inactivated by utilizing the LP UV lamp. Generally, applying higher UV doses resulted in higher log inactivation of *E. coli*.

- It was shown that by increasing the concentration of humic acid and kaolinite, the log inactivation of *E. coli* reduced. Moreover, results indicated that by applying the same UV doses in different sample depths with the same optical properties, as the sample depth increased, the inactivation rate decreased, resulting in a lower log inactivation of pathogens. Finally, the GLM analysis for *E. coli* inactivation rate at sample depth of 4 cm determined that UV disinfection performance was significantly influenced by turbidity, absorbance, and the interaction between these two parameters (p-value < 0.05).

- By calculating the corrected applied UV doses, the *E. coli* inactivation curve followed a first-order linear relation characterized by an inactivation rate constant of 0.67 cm^2/mJ. Furthermore, the normal probability plot for sample depth of 4 cm from analyzing the results indicated that the accuracy of corrected applied UV doses for *E. coli* inactivation would be affected without considering the phenomena related to scattering of light in the correction factors.

- The comparison between relative corrected UV doses and relative inactivation rate constants obtained according to the GLM determined that as turbidity increased up to 10 NTU, the applied correction factors overestimated the UV doses. It could be concluded that an additional correction factor is required to account for light

scattering. However, the CB apparatus modeling results were not accurate enough to draw a conclusion by comparing the average germicidal irradiance with the one obtained from experiments.

- UV disinfection reactor was simulated using a CFD software based on a flow model and a radiative transfer model coupled with the *E. coli* inactivation kinetics model obtained from the experiments using CB apparatus in this study and MS2 inactivation kinetics model obtained from experiments carried out by Baldasso (2020) to determine the predicted log inactivation for both pathogens under the effect of optical properties.

- The results of the UV disinfection reactor modeling for *E. coli* indicated that the UV doses in the reactor were high enough to disinfect microorganisms in case of different flowrates and optical properties. The predicted MS2 log inactivation results determined the significance of absorbance and insignificance of turbidity, which was consistent with the findings of experimental results obtained by Baldasso (2020) and Batch et al. (2004). Moreover, the comparison between the predicted MS2 log inactivation and the one obtained from field experiments indicated that the CFD simulations were able to effectively predict MS2 inactivation.

Based on the results from this study, as the correction factors proposed by Bolton and Linden (2003) were not sufficient to calculate the effective UV doses in a turbid but not absorbing sample and as the CB apparatus modeling results were not accurate enough, it would be beneficial to conduct a further study on the CB apparatus modeling. In this case, since CFD is a powerful tool for predicting radiation transfer if finely tuned, it is proposed to perform the simulations with a smaller setup, improve the description of the glass, and consider different values for angular discretization in the radiation model to obtain a precise average UV irradiance throughout the sample. Then it would be possible to determine another correction factor, considering the scattering effect caused by turbidity.

In conclusion, removing suspended and dissolved substances to prevent increasing turbidity and absorbance from water and wastewater is essential to enhance UV disinfection performance for inactivating pathogens in water and wastewater treatment. In addition, a proper flowrate control based on on-line measurement could be an effective tool.

REFERENCES

Azimi, Y., Allen, D., & Farnood, R. (2012). Kinetics of UV inactivation of wastewater bioflocs. *Water Research*, *46*(12), 3827-3836.

Baldasso, V. (2020). UV disinfection for low-income communities: performance analysis. *http://hdl.handle.net/10589/164617*

Batch, L. F., Schulz, C. R., & Linden, K. G. (2004). Evaluating water quality effects on UV disinfection of MS2 coliphage. *Journal-American Water Works Association*, *96*(7), 75-87.

Beck, S. E., Wright, H. B., Hargy, T. M., Larason, T. C., & Linden, K. G. (2015). Action spectra for validation of pathogen disinfection in medium-pressure ultraviolet (UV) systems. *Water Research, 70*, 27-37.

Besaratinia, A., Yoon, J. i., Schroeder, C., Bradforth, S. E., Cockburn, M., & Pfeifer, G. P. (2011). Wavelength dependence of ultraviolet radiation-induced DNA damage as determined by laser irradiation suggests that cyclobutane pyrimidine dimers are the principal DNA lesions produced by terrestrial sunlight. *The FASEB Journal*, *25*(9), 3079-3091.

Betancourt, W. Q., & Rose, J. B. (2004). Drinking water treatment processes for removal of Cryptosporidium and Giardia. *Veterinary parasitology*, *126*(1-2), 219-234.

Bolton, J., & Cotton, C. (2008). Mechanism of UV disinfection. *The Ultraviolet Disinfection Handbook, American Water Works Association, Denver, CO*, 25-40.

Bolton, J. R. (2010). Ultraviolet Applications Handbook.

Bolton, J. R., & Linden, K. G. (2003). Standardization of methods for fluence (UV dose) determination in bench-scale UV experiments. *Journal of environmental engineering*, *129*(3), 209-215.

Bolton, J. R., Stefan, M. I., Shaw, P.-S., & Lykke, K. R. (2011). Determination of the quantum yields of the potassium ferrioxalate and potassium iodide–iodate actinometers and a method for the calibration of radiometer detectors. *Journal of Photochemistry and Photobiology A: Chemistry*, *222*(1), 166-169.

Cantwell, R. E., & Hofmann, R. (2008). Inactivation of indigenous coliform bacteria in unfiltered surface water by ultraviolet light. *Water Research*, *42*(10-11), 2729-2735.

Cantwell, R. E., Hofmann, R., & Templeton, M. R. (2008). Interactions between humic matter and bacteria when disinfecting water with UV light. *Journal of applied microbiology*, *105*(1), 25-35.

Chawla, S., Parashar, R., & Parashar, R. (2015). Is estimation of residual free chlorine in water by drop number titration method reliable? Investigation of statistical, pragmatic, psychological and philosophical reasons. *Int. J. Chem. Pharm. Rev. Res*, *2*(1), 11-18.

Chick, H. (1908). An investigation of the laws of disinfection. *Epidemiology & Infection*, *8*(1), 92-158.

Choi, Y., & Choi, Y.-j. (2010). The effects of UV disinfection on drinking water quality in distribution systems. *Water Research*, *44*(1), 115-122.

Christensen, J., & Linden, K. G. (2003). How particles affect UV light in the UV disinfection of unfiltered drinking water. *Journal-American Water Works Association*, *95*(4), 179-189.

Crittenden, J. C., Trussell, R. R., Hand, D. W., Howe, K. J., & Tchobanoglous, G. (2012). *MWH's Water Treatment: Principles and Design*. John Wiley & Sons.

Dieter, G. E., & Schmidt, L. C. (2009). *Engineering design*. McGraw-Hill Higher Education Boston.

Dotson, A. D., Rodriguez, C. E., & Linden, K. G. (2012). UV disinfection implementation status in US water treatment plants. *Journal-American Water Works Association*, *104*(5), E318-E324.

Emerick, R. W., Loge, F. J., Thompson, D., & Darby, J. L. (1999). Factors influencing ultraviolet disinfection performance part II: association of coliform bacteria with wastewater particles. *Water environment research*, *71*(6), 1178-1187.

Farrell, C., Hassard, F., Jefferson, B., Leziart, T., Nocker, A., & Jarvis, P. (2018). Turbidity composition and the relationship with microbial attachment and UV inactivation efficacy. *Science of the total environment*, *624*, 638-647.

Gelete, G., Gokcekus, H., Ozsahin, D. U., Uzun, B., & Gichamo, T. (2020). Evaluating disinfection techniques of water treatment. *Desalination and Water Treatment*, *177*, 408-415.

Goosen, N., & Moolenaar, G. F. (2008). Repair of UV damage in bacteria. *DNA repair*, *7*(3), 353-379.

Gray, N. F. (2014). Ultraviolet Disinfection. In *Microbiology of Waterborne Diseases* (pp. 617-630). Elsevier.

Henao, L. D., Cascio, M., Turolla, A., & Antonelli, M. (2018). Effect of suspended solids on peracetic acid decay and bacterial inactivation kinetics: experimental assessment and definition of predictive models. *Science of the total environment*, *643*, 936-945.

Hess-Erga, O.-K., Attramadal, K. J. K., & Vadstein, O. (2008). Biotic and abiotic particles protect marine heterotrophic bacteria during UV and ozone disinfection. *Aquatic Biology*, *4*(2), 147-154.

Hijnen, W., Beerendonk, E., & Medema, G. J. (2006). Inactivation credit of UV radiation for viruses, bacteria and protozoan (oo) cysts in water: a review. *Water Research*, *40*(1), 3-22.

Ho, C. (2009). Evaluation of reflection and refraction in simulations of ultraviolet disinfection using the discrete ordinates radiation model. *Water science and technology*, *59*(12), 2421-2428.

Hoyer, O. (1998). Testing performance and monitoring of UV systems for drinking water disinfection. *Water Supply*, *16*(1), 424-429.

Hoyer, O. (2004). Water disinfection with UV radiation–requirements and realization. *Proceedings of the European conference UV Karlsruhe, UV radiation. Effects and technologies*.

Hu, J., Chu, X., Quek, P., Feng, Y., & Tan, X. (2007). Inactivation of particle-associated viruses by UV. *Journal of Water Supply: Research and Technology—AQUA*, *56*(6-7), 393-397.

Hu, J., & Quek, P. H. (2008). Effects of UV radiation on photolyase and implications with regards to photoreactivation following low-and medium-pressure UV disinfection. *Applied and Environmental Microbiology*, *74*(1), 327-328.

Huber, S. A., Balz, A., Abert, M., & Pronk, W. (2011). Characterisation of aquatic humic and non-humic matter with size-exclusion chromatography–organic carbon detection–organic nitrogen detection (LC-OCD-OND). *Water Research*, *45*(2), 879-885.

Jin, S., Mofidi, A. A., & Linden, K. G. (2006). Polychromatic UV fluence measurement using chemical actinometry, biodosimetry, and mathematical techniques. *Journal of environmental engineering*, *132*(8), 831-841.

Kheyrandish, A., Mohseni, M., & Taghipour, F. (2018). Protocol for determining ultraviolet light emitting diode (UV-led) fluence for microbial inactivation studies. *Environmental science & technology*, *52*(13), 7390-7398.

Knudson, G. B. (1985). Photoreactivation of UV-irradiated Legionella pneumophila and other Legionella species. *Applied and Environmental Microbiology*, *49*(4), 975-980.

Kollu, K., & Örmeci, B. (2012). Effect of particles and bioflocculation on ultraviolet disinfection of Escherichia coli. *Water Research*, *46*(3), 750-760.

Kuhn, H., Braslavsky, S., & Schmidt, R. (2004). Chemical actinometry (IUPAC technical report). *Pure and Applied Chemistry*, *76*(12), 2105-2146.

Li, M., Qiang, Z., Bolton, J. R., & Ben, W. (2012). Impact of reflection on the fluence rate distribution in a UV reactor with various inner walls as measured using a micro-fluorescent silica detector. *Water Research*, *46*(11), 3595-3602.

Li, W., Li, M., Bolton, J. R., Qu, J., & Qiang, Z. (2017). Impact of inner-wall reflection on UV reactor performance as evaluated by using computational fluid dynamics: The role of diffuse reflection. *Water Research*, *109*, 382-388.

Liu, G., Ling, F., Magic-Knezev, A., Liu, W.-T., Verberk, J., & Van Dijk, J. (2013). Quantification and identification of particle-associated bacteria in unchlorinated drinking water from three treatment plants by cultivation-independent methods. *Water Research*, *47*(10), 3523-3533.

Liu, G., Slawson, R. M., & Huck, P. M. (2007). Impact of flocculated particles on low pressure UV inactivation of E. coli in drinking water. *Journal of Water Supply: Research and Technology—AQUA*, *56*(3), 153-162.

Liu, W.-j., & Zhang, Y.-j. (2006). Effects of UV intensity and water turbidity on microbial indicator inactivation. *Journal of Environmental Sciences*, *18*(4), 650-653.

Malayeri, A. H., Mohseni, M., Cairns, B., Bolton, J. R., Chevrefils, G., Caron, E., Barbeau, B., Wright, H., & Linden, K. G. (2016). Fluence (UV dose) required to achieve incremental log inactivation of bacteria, protozoa, viruses and algae. *IUVA News*, *18*(3), 4-6.

Malley Jr, J. (2000). Engineering of UV disinfection systems for drinking water. *IUVA News*, *2*(3), 8-14.

Mamane-Gravetz, H., & Linden, K. G. (2005). Relationship between physiochemical properties, aggregation and uv inactivation of isolated indigenous spores in water. *Journal of applied microbiology*, *98*(2), 351-363.

Mamane, H. (2008). Impact of particles on UV disinfection of water and wastewater effluents: a review. *Reviews in Chemical Engineering*, *24*(2-3), 67-157.

Mamane, H., & Linden, K. G. (2006). Impact of particle aggregated microbes on UV disinfection. II: Proper absorbance measurement for UV fluence. *Journal of environmental engineering*, *132*(6), 607-615.

Metcalf, L., Eddy, H. P., & Tchobanoglous, G. (2003). *Wastewater engineering: treatment, disposal, and reuse* (Vol. 4). McGraw-Hill New York.

Munoz, A., Craik, S., & Kresta, S. (2007). Computational fluid dynamics for predicting performance of ultraviolet disinfection sensitivity to particle tracking inputs. *Journal of Environmental Engineering and Science*, *6*(3), 285-301.

Oguma, K., Izaki, K., & Katayama, H. (2013). Effects of salinity on photoreactivation of Escherichia coli after UV disinfection. *Journal of water and health*, *11*(3), 457-464.

Oguma, K., Katayama, H., & Ohgaki, S. (2002). Photoreactivation of Escherichia coli after low-or medium-pressure UV disinfection determined by an endonuclease sensitive site assay. *Applied and Environmental Microbiology*, *68*(12), 6029-6035.

Orta de Velasquez, M. T., Rojas-Valencia, M. N., & Ayala, A. (2008). Wastewater disinfection using ozone to remove free-living, highly pathogenic bacteria and amoebae. *Ozone: Science and Engineering*, *30*(5), 367-375.

Passantino, L., Malley Jr, J., Knudson, M., Ward, R., & Kim, J. (2004). Effect of low turbidity and algae on UV disinfection performance. *Journal-American Water Works Association*, *96*(6), 128-137.

Pirnie, M., Linden, K. G., Malley, J. P., Schmelling, D., & USA, O. o. W. (2006). *Ultraviolet disinfection guidance manual for the final long term 2 enhanced surface water treatment rule: EPA 815-R-06-007*. EPA.

Qiang, Z., Li, W., Li, M., Bolton, J. R., & Qu, J. (2015). Inspection of Feasible Calibration Conditions for UV Radiometer Detectors with the KI/KIO 3 Actinometer. *Photochemistry and Photobiology*, *91*(1), 68-73.

Rahn, R. O. (1997). Potassium iodide as a chemical actinometer for 254 nm radiation: use of Iodate as an electron scavenger. *Photochemistry and Photobiology*, *66*(4), 450-455.

Ran, Z., Wang, Z., Yao, M., & Li, S. (2019). Study on the Inactivation of E. coli in Water by UV-LED. International Conference on Sustainable Development of Water and Environment,

Reed, N. G. (2010). The history of ultraviolet germicidal irradiation for air disinfection. *Public health reports*, *125*(1), 15-27.

Rodriguez, R. A., Bounty, S., Beck, S., Chan, C., McGuire, C., & Linden, K. G. (2014). Photoreactivation of bacteriophages after UV disinfection: Role of genome structure and impacts of UV source. *Water Research*, *55*, 143-149.

Rosenblum, J., Ge, C., Bohrerova, Z., Yousef, A., & Lee, J. (2012). Ozonation as a clean technology for fresh produce industry and environment: sanitizer efficiency and wastewater quality. *Journal of applied microbiology*, *113*(4), 837-845.

Rubio, D., Nebot, E., Casanueva, J., & Pulgarin, C. (2013). Comparative effect of simulated solar light, UV, UV/H2O2 and photo-Fenton treatment (UV–Vis/H2O2/Fe2+, 3+) in the Escherichia coli inactivation in artificial seawater. *Water Research*, *47*(16), 6367-6379.

Sinha, R. P., & Häder, D.-P. (2002). UV-induced DNA damage and repair: a review. *Photochemical & Photobiological Sciences*, *1*(4), 225-236.

Sommer, R., Haider, T., Cabaj, A., Pribil, W., & Lhotsky, M. (1998). Time dose reciprocity in UV disinfection of water. *Water science and technology*, *38*(12), 145-150.

Sommer, R., Lhotsky, M., Haider, T., & Cabaj, A. (2000). UV inactivation, liquid-holding recovery, and photoreactivation of Escherichia coli O157 and other pathogenic Escherichia coli strains in water. *Journal of food protection*, *63*(8), 1015-1020.

Song, K., Mohseni, M., & Taghipour, F. (2016). Application of ultraviolet light-emitting diodes (UV-LEDs) for water disinfection: A review. *Water Research*, *94*, 341-349.

Sousa, J. M., Macedo, G., Pedrosa, M., Becerra-Castro, C., Castro-Silva, S., Pereira, M. F. R., Silva, A. M., Nunes, O. C., & Manaia, C. M. (2017). Ozonation and UV254 nm radiation for the removal of microorganisms and antibiotic resistance genes from urban wastewater. *Journal of hazardous materials*, *323*, 434-441.

USEPA (2006). Ultraviolet disinfection guidance manual for the final long term 2 enhanced surface water treatment rule. *https://nepis.epa.gov/Exe/ZyPURL.cgi?Dockey=60000T3.txt*

Templeton, M., Hofmann, R., & Andrews, R. (2006). UV inactivation of humic-coated bacteriophages MS2 and T4 in water. *Journal of Environmental Engineering and Science*, *5*(6), 537-543.

Watson, H. E. (1908). A note on the variation of the rate of disinfection with change in the concentration of the disinfectant. *Epidemiology & Infection*, *8*(4), 536-542.

WHO, G. (2011). Guidelines for drinking-water quality. *World Health Organization*, *216*, 303-304.

Wolfe, R. L. (1990). Ultraviolet disinfection of potable water. *Environmental science & technology*, *24*(6), 768-773.

Wu, Y., Clevenger, T., & Deng, B. (2005). Impacts of goethite particles on UV disinfection of drinking water. *Applied and Environmental Microbiology*, *71*(7), 4140-4143.

Xi, J., Zhang, F., Lu, Y., & Hu, H.-Y. (2017). A novel model simulating reclaimed water disinfection by ozonation. *Separation and Purification Technology*, *179*, 45-52.

Zhai, H., He, X., Zhang, Y., Du, T., Adeleye, A. S., & Li, Y. (2017). Disinfection byproduct formation in drinking water sources: a case study of Yuqiao reservoir. *Chemosphere*, *181*, 224-231.

Zimmer, J., & Slawson, R. (2002). Potential repair of Escherichia coli DNA following exposure to UV radiation from both medium-and low-pressure UV sources used in drinking water treatment. *Applied and Environmental Microbiology*, *68*(7), 3293-3299.